Numerical Investigation on Heat Transfer in a Compact Linear Fresnel Reflector (CLFR) Receiver

Dissertation—II

Submitted in partial fulfillment of the requirement for the award of degree of

Master of Technology

in

Mechanical Engineering

by

Rohit Duggal

Regd. No: 11510247

Under the guidance of

Dr. Ravindra Jilte

U.ID: 20336

DEPARTMENT OF MECHANICAL ENGINEERING

LOVELY PROFESSIONAL UNIVERSITY

PUNJAB

2016-2017

CERTIFICATE

I hereby certify that the work being presented in the dissertation entitled "***Numerical Investigation on Heat Transfer in a Compact Linear Fresnel Reflector (CLFR) Receiver"*** in partial fulfilment of the requirement of the award of the Degree of master of technology and submitted to the Department of Mechanical Engineering of Lovely Professional University, Phagwara, is an authentic record of my own work carried out under the supervision of Dr. Ravindra Jilte, Professor Department of Mechanical Engineering, Lovely Professional University. The matter embodied in this dissertation has not been submitted in part or full to any other University or Institute for the award of any degree.

Date:

Name: Rohit Duggal

Registration No: 11510247

This is to certify that the above statement made by the candidate is correct to the best of my knowledge.

Date:

Name: Dr. Ravindra Jilte

UID: 20336

COD: Sudhanshu Dogra

The external viva-voce examination of the student was held successfully on

Signature of Examiner

DECLARATION

I, Rohit Duggal, student of **Master of Technology (Mechanical Engineering)** under School of **Mechanical Engineering** of Lovely Professional University, Punjab, hereby declare that all the information furnished in this dissertation reports based on my own intensive research and is genuine. This dissertation does to the best of my knowledge, contain part of my work which has been submitted for the award of my degree either of this university without proper citation.

Rohit Duggal
Registration No. 11510247

Date:

ACKNOWLEDGMENT

First and the foremost I offer my sincerest gratitude to my supervisor, **Dr. Ravindra Jilte,** Professor, School of Mechanical Engineering, Lovely Professional University, Punjab.

I am thankful to **Mr. Gurpreet Singh Phull**, (HOS) and **Mr. Sudhanshu Dogra** (HOD) School of Mechanical Engineering, Lovely Professional University, Punjab.

I would like to thank all the staff members of School of Mechanical engineering who have been very patient and co-operative with me.

I would also like to extend my gratitude to my seniors.

I would like to thank **Lovely Professional University** for giving me opportunity to use their resources and work in such a challenging environment. I am grateful to the individuals whom contributed their valuable time towards my thesis.

Last but not the least, I express my sincere gratitude to my parents and brother who have always supported me throughout all my studies at university and encouraged me with their best wishes.

ABSTRACT

Solar energy in particular has been receiving increasing attention due to the substantial solar insolation levels in India all year round. This makes India an ideal destination for LFR development and deployment as an exemplary solar technology. Therefore, this thesis will attempt to offer and analyses novel LFR designs as a contribution to the ongoing efforts to design, improve, characterize, build, test, and demonstrate LFR solar collector systems. Further, to optimize different parameters within concentrator geometry in order to achieve high optical efficiency. This research proposed the development of an innovative three-dimensional medium concentrating design, which captured a large part of the diffuse solar radiation in addition to the direct component. The study finds its usefulness in solar thermal power plant wherein thermal losses plays the important role in optimizing the plant. In case of solar thermal power plant based on CSP (i.e. concentrated solar plant) the operating temperatures are higher causing the higher heat losses (convective and radiative). Among various solar thermal technologies present such as dish concentrating, parabolic trough technologies, Compact Linear Fresnel Reflector (CLFR) proves to be efficient and simple method to exploit solar energy. Therefore, the present work is undertaken to study the of CLFR receiver and its associated losses.

Table of Contents

Index of Tables

Index of Figures

Nomenclature

A	Area, m^2
C	Concentration Ratio
CFD	Computational Fluid Dynamics
CLFR	Compact Linear Fresnel Reflector
CPC	Compound Parabolic Concentrator
CPV	Concentrating Photovoltaic
CR	Concentration Ratios
CSP	Concentrating Solar Power
CST	Concentrating Solar Technology
DNI	Direct Normal Irradiance
DSG	Direct Steam Generation
ETC	Evacuated Tube Collector
FPC	Flat Plate Collector
G	Irradiance, W/m^2
g	acceleration due to gravity, m/s^2
GW	Gigawatt
h	Heat Transfer Coefficient, W/m^2K
HFC	Heliostat Field Collector
HTF	Heat Transfer Fluid
IEA	International Energy Agency
k	Thermal Conductivity, W/mK
L	effective length, m
LFC	Linear Fresnel Collector
LFR	Linear Fresnel Reflector
m	mass flow rate, kg/s
MW	Megawatt
NPS	Nominal Pipe Size
Nu	Nusselt Number
P	Pressure, N/m^2
PDR	Parabolic Dish Reflector
PT	Parabolic Trough
PTC	Parabolic Trough Collector
PV	Photovoltaic
Q	Heat Transfer, W
R	Resistance, K/W
Re	Reynolds Number
SEGS	Solar Electric Generating Systems
SHP	Solar Heat and Power
SPLFR	Semi-parabolic Linear Fresnel Reflector
SS	Stainless steel
t	Time, sec
T	Temperature, K
TES	Thermal Energy Storage
u	velocity in x-direction, m/s
V	View factor
v	velocity in y-direction, m/s
w	velocity in z-direction, m/s

Subscript

sys	system
o	optical
g	geometrical
re	receiver
su	surrounding
r	receiver surface
c	collector
cond	conductance
conv	convective
out	outflow
in	inflow
th	thermal

Greek symbols

η	efficiency
ε	emissivity
α	thermal diffusivity, m^2/s
ρ	density, kg/m^3
β	inverse differential temperature, K^{-1}
ν	kinematic viscosity, kg/m^3
σ	Stefann Boltzmann constant, 5.67×10^{-8} W/m^2K^4

CHAPTER-1

1 Introduction

Concentrating solar power (CSP) system is used to produce useful energy forms (i.e. heat, electricity or fuels), through various downstream technologies, by concentrating direct beam solar radiation with the help of combination of lens or mirrors.

1.1 History and context

The first surge of commercialization in CSP technology was between 1984 and 1995, that stopped until 2005, in spite of various research and development activities. Since then, total installed capacity however lesser than Photovoltaic (PV) has gained momentum, provided commercialization of technology is decade or so behind [1].

Solar energy has been an interesting topic throughout history [2]. For example:

- Archimedes proposed to concentrate sun with an idea of mirrored panels in around 200 BC;
- The Greek mathematician Diocles, in 2nd century BC, described the optical properties of a parabolic trough.
- Even the heliostat designs development as was explained in 1746 by Comte de Buffon.
- Universal exhibition (Paris) saw demonstrations for a dish driven steam engine technology developed by Augustin Mouchot.
- In 1913, Frank Schuman made a historical landmark with successful pumping system operated using Parabolic Trough (PT) technology in Egypt.
- In 1980, California gave birth to CSP as an industry along with governmental policies which led to constructing 9 separate PT based ‘Solar Electric Generating Systems’ (SEGS), with 354 MW capacity. Oil as heat transfer fluid and steam turbines for power marked the technology for trough receivers.

Since each new technology has to face investment cost trouble so is CSP through the use of high economy steam turbines and capital cost etc. However, there are reasons for CSP development [3]:

- The 10th CSP plant fled into loss due to policy changes however, concern over climate change has forced the policy makers dominating the political agenda over power supply.

- Since being a potential technology is making a quick and large cut downs in greenhouse gas emissions, it has seen a resurgence in development from 2005.
- The growth led by Spain with tariff incentives and integrating with thermal storage has made solar energy distributable. Various countries with CSP projects include Australia, China, Cyprus, Greece, India, Italy, Malta, Middle East (Egypt, Israel), North Africa (Algeria, Morocco), South Africa and Portugal (both installed and under construction).
- In 2010, India, with its Jawaharlal Nehru National Solar Mission targeted 20 GW of PV and CSP to be installed by 2022.

CSP versus PV [2][4]:

- Presently installed PV capacity is ten times greater than CSP due to 15 years of deployment shift. Hence, CSP has to see the cost reduction which PV has significant observed. Moreover, PV is affordable in case of non-dispatchable power production for its most applications.
- Therefore, the circumstances have led to greater attention towards CSP's potential advantages. The advantages of dispatchability and built-in thermal energy storage along with non-electrical applications (fuels)

1.2 Approaches to concentrating solar power (CSP)

Presently the technology configurations that are in commercial level are:

- Parabolic Trough (PT)
- Central Receiver Tower
- Linear Fresnel Reflector (LFR)
- Fresnel lenses (for Concentrating Photovoltaic (CPV))
- Parabolic Dish Technology

In addition to these concepts, Solar Furnace arrangement is extensively used as a research tool. A solar furnace basically consists of a mounted fixed-orientation parabolic dish with heliostats (one or more external heliostats) concentrating solar radiation at a fixed angle.

1.3 Parabolic trough

In this configuration parabolic trough-shaped mirrors are used. These produce a linear focus along receiver tube as that of parabola's focal line as shown in Figure 1.1. This results in lateral movements of focal line constantly remaining on receiver tubes. Trough systems using thermal energy collection via evacuated tube receivers are currently the most widely deployed CSP technology. In this configuration, an oil heat transfer fluid is usually used to collect the heat from the receiver tubes and transport it to a central power block.

Figure 1.1. Parabolic trough collector Nevada Solar 1 [4].

1.4 Central receiver tower

This is a two axis tracking system. It involves large mirrors with array of heliostats that focus solar light on to a fixed receiver mounted on a tower top as illustrated in Figure 1.2. It is a sophisticated system, since efficient energy conversions are achieved at a single large point of receiver [5]. Being a point focus technology, higher concentration ratios (CR) are possible as compared to linear focusing counterparts. This allows higher temperature operations with lower losses.

Figure 1.2. Central receiver tower plant Gemasolar plant [5].

1.5 Linear Fresnel reflectors

Linear Fresnel reflector (LFR), as shown in Figure 1.3, a downward facing receiver gets a linear focus from array of mirrors mounted on ground. Single axis independent movement of curved or straight mirrors is an advantage. For thermal systems serves two purposes a) avoids rotational joints b) reduced convective losses (single downward facing receiver configuration). The advantages associated:

- Its simple design with almost flat mirrors
- Less supporting structure

outweighs the cons of lower overall thermal and optical efficiency [6]. Compact Linear Fresnel Reflectors (CLFRs) exploit multiple receivers (increasing thermal efficiency) for each set of mirrors (increasing optical efficiency). In this way adjacent mirrors can have different inclinations for different receivers allowing for higher packing density of mirrors. This in turn increases optical efficiency and thereby minimizing land use.

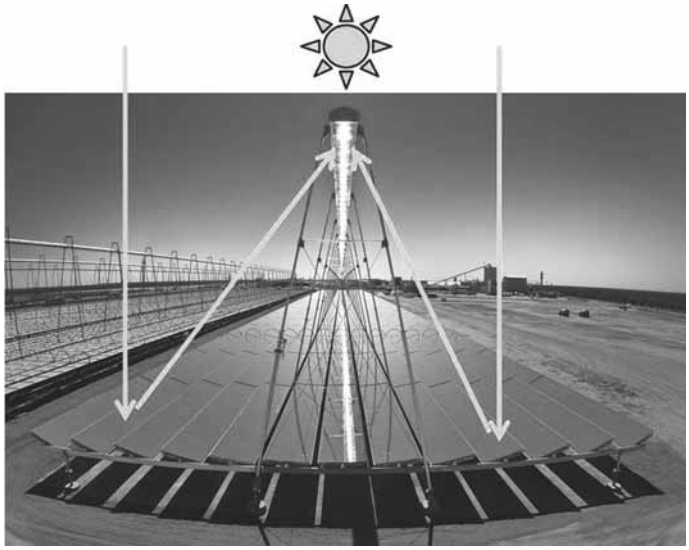

Figure 1.3. Linear Fresnel reflector multiple mirror [6].

1.6 Fresnel lens

A large scale conventional lens is expensive and even not practical to materialize. The Fresnel lens, on the contrary, is made as a series of concentric small steps [7]. All the steps together with small thickness provides a surface shape similar to conventional lens as shown in Figure 1.4. This is a point focus system which requires two-axis for accurate sun tracking.

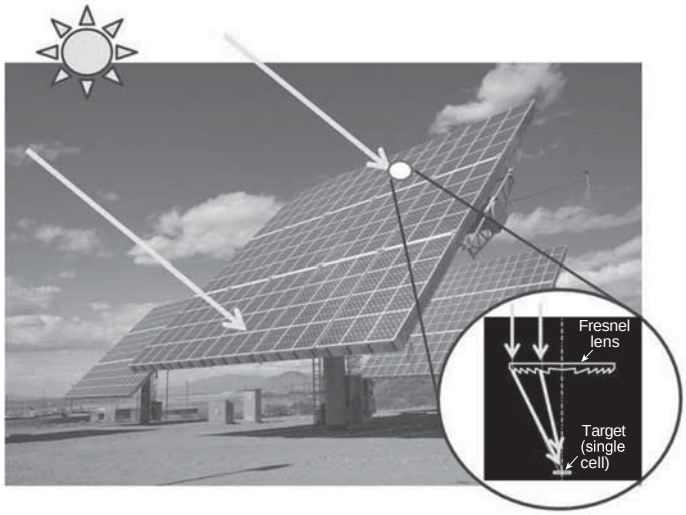

Figure 1.4. Fresnel lens-based CPV: multiple small units on a heliostat [7].

1.7 Parabolic dishes

This is a type of point focus system in which paraboloid dish concentrates solar radiation as shown in Figure 1.5. Dish systems, like troughs, exploit the geometric properties of a parabola, but as a

three-dimensional exploiting geometric properties of parabola (operating temperature over 1000°C). Dish systems, offers full aperture towards sun thereby offering the highest potential solar conversion efficiencies among all the CSP technologies [8]. They are however face the commercialization issue being demonstrated up to 24m dish. Even micro dishes (diameter of centimeters) is established for maximum thermal conversion.

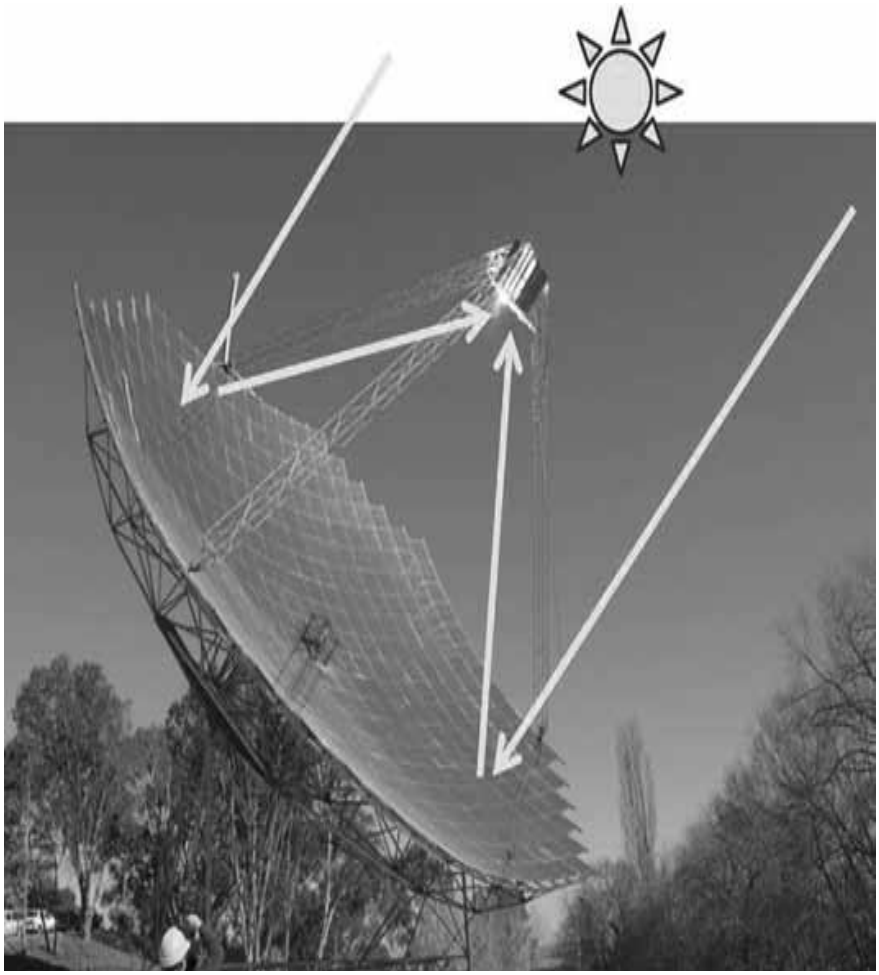

Figure 1.5. Paraboloidal dish concentrator: tracks the sun in two axes [8].

1.8 Future growth, cost and value

The capital cost of CSP systems is what presently researchers and technology developers are working upon since there

Various cost reduction paths for CSP [9]:

- A study for the Global Environment Facility comprehensive scenario predicted 5GW by 2015 Figure 1.6 [10].

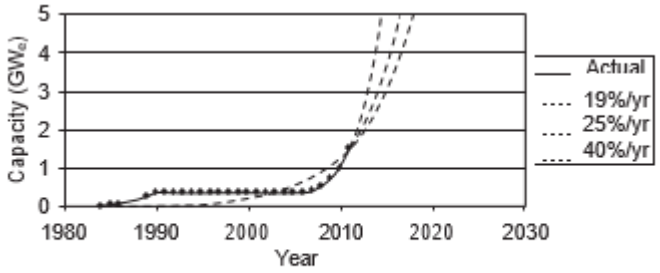

1.6 Global installed capacity of CSP plants, both actual and possible future compound growth rates.

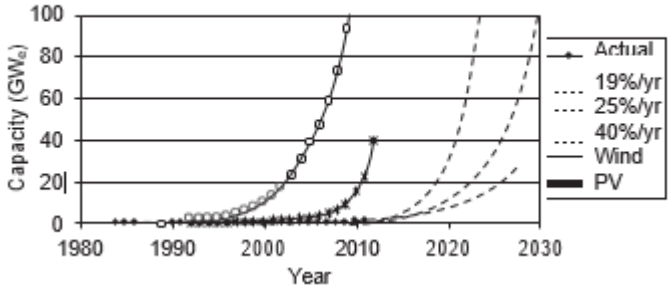

Figure 1.6. Global installed capacity of CSP plants, growth rates wind and PV [9].

The International Energy Agency (IEA) predicted cost reduction up to 25% by 2050 for CSP technology [11].

- Spanish as well as European CST industry commissioned [12] to study cost energy feasibility on economic basis. A reduction in 40-50 % is expected by reducing cost of manufacturing and increasing annual output. The potential is expected to reach 100 GW in installed capacity referring to policy measures.

Some relevant studies regarding cost reduction for example as done [13] for linear focus and [14] for tower system estimates a total reduction of 40% and 50% respectively.

The importance is laid of thermal energy storage that it can be 30% or more valuable than current average market values [15], [16].

CHAPTER-II

2 Terminology

2.1 Fundamental principles of concentrating solar power systems

Schematic of a concentrating solar power (CSP) system is illustrated in Figure 2.1. Line focusing and point focusing system differ from each other on the basis of ability to concentrate solar flux of some 50-100 times for linear and 500 to thousands for point focus systems [2].

A receiver must be subjected to focussed radiation to convert into other form may be thermal.

Basically, the currently situation is [17]:

- Trough-based CSP systems use concentric tubes one with working fluid and the other as covering made of glass typically having vacuum in the annular space to reduce convective losses.
- Further, as a modification and advantageous for compactness. The system, with multiple tube arrangement in different cavity shapes, is developed in both point focus and line focus systems.
- Moreover, Direct or volumetric absorption technology receivers are commercialized. It

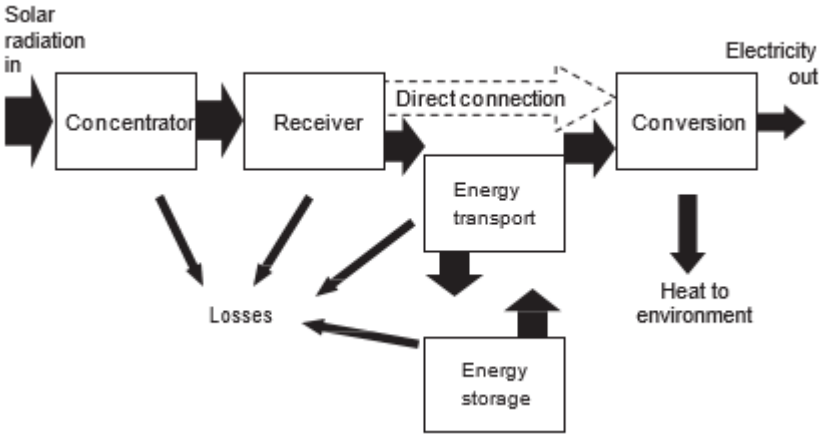

Figure 2.1. Schematic of the solar thermal power system [2].

consists of surfaces that are immersed in heat transfer fluid to absorb radiation.

There lefts options with the energy [18], [19]:

- To be converted directly to electricity (desired form) as Stirling engines, solid state semiconductors and thermoelectric conversion devices are accommodated as an integral part to the receiver.
- Or dispatched to final target for further conversions using heat transfer fluid (HTF)/thermal energy storage (TES) medium (collected energy can be dispatched to other places)

The final step in a CSP system is power production. The dominant approach here is steam turbines [20]:

- Stirling engines
- organic Rankine cycles
- Brayton cycles

The overall efficiency of CSP system is product of individual sub-system efficiencies i.e. concentrator, transport, optical receiver, conversion and storage) [20].

$$\eta_{sys} = \eta_{optical} \times \eta_{receiver} \times \eta_{storage} \times \eta_{transport} \times \eta_{conversion} \quad (1.1)$$

2.2 Concentrating optics

2.3 Solar radiation

Since sun (5760 K surface temperature) can be assumed as a black body radiation source with its temperature as 5200 K because of selective absorption of wavelength in atmosphere [21]. This radiation is of two types:

- Direct Normal Irradiance (DNI)
- Diffuse or Scattered radiation

CSP systems use DNI component of solar radiation. Direct normal irradiance (DNI) is defined as the flux density (Insolation/radiant flux/irradiance) of un-scattered sunlight. This is measured on a flat plane perpendicular to the solar radiation. The value 2011 1367 W/m^2 is solar constant [22]. This is defined as intensity of solar radiation on plane in outer atmosphere of earth. Another parameter is concentration ratio which is heart of CSP as it amplifies radiation to higher intensity [23].

- The optical concentration ratio, C_o

- The geometric concentration ratio, C_g

C_o is the fraction of receiver surface irradiance (G_r) to the incident solar irradiance (G):

$$C_o = \frac{G_r}{G} \quad (1)$$

It may be defined at any position of an output flux distribution. However, special reference is given to the point of highest light intensity and peak concentration ratio of a flux distribution.

C_g is expressed as the ratio of aperture area of collector (A_c) to area of the receiver (A_r):

$$C_g = \frac{A_c}{A_r} \quad (2)$$

"Number of suns" is also referred to define concentration ratio. For example, a geometric concentration ratio of 1,300 would be called as '1,300 suns'. Hence, it would result to 1.3 MW/m^2 for an assumed solar flux of 1,000 W/m^2 at the surface of the receiver. Moreover, the sun position can be precisely tracked with equations developed already for both linear as well as point focus systems.

2.4 Secondary optics

Degree of concentration up to 80-90% of thermodynamic limit in case of configurations Figure 2.2 like Trombe-Meinel cusp, Compound Parabolic Concentrator (CPC) , Mouchot conical mirror etc [17].

Figure 2.2. A secondary Trombe-Meinel cusp concentrator [17].

2.5 Losses from receivers

The steady heat equilibrium equation is energy inflow equals energy outflow. Losses will also be considered. This follows as:

$$Q_{cond} + Q_{conv} + Q_{re} + Q_r = Q_{loss} \quad (3)$$

The receiver energy efficiency is the ratio of usefully converted energy to the energy intercepted.

$$\eta_{re} = \frac{Q_{out}}{Q_{in}} = \frac{Q_{in} - Q_{loss}}{Q_{in}} \quad (4)$$

where for the receiver

$$Q_{in} = \int_{time}^{t} \int_{aperture}^{s} G_{incident}(t) dA\, dt \quad (5)$$

Stagnation temperature is obtained when there is no output energy and receiver gets heated up continuously.

2.6 Radiative losses

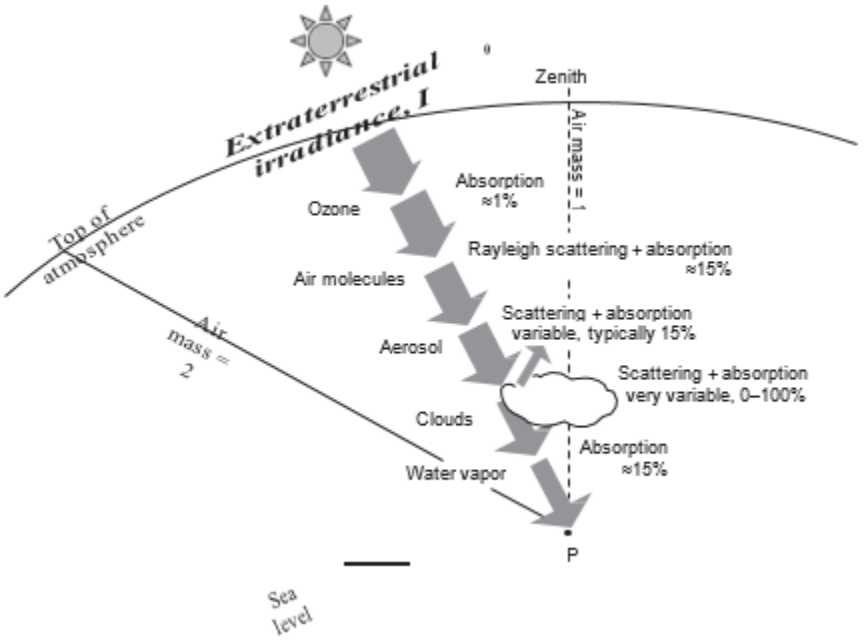

Figure 2.3. Influencing solar radiation three components [24].

Any surface that is at higher temperature than absolute zero emits radiation. Thus, radiative losses include the net radiation emitted (receiver geometry driven) from high temperature walls of receivers. The reflection losses (if glass aperture is involved) Figure 2.3 of the incident solar flux through concentrator. Anti-reflective coating or the assumption of real surfaces to be modelled as

grey bodies (i.e. a constant emissivity across all wavelengths) prevent these kind of losses. Selective absorbing surfaces have high absorptivity (for solar radiation wavelength) and a low emissivity (for infrared radiation from high temperature surface). The radiation shape/view factors are used to determine radiation losses [24].

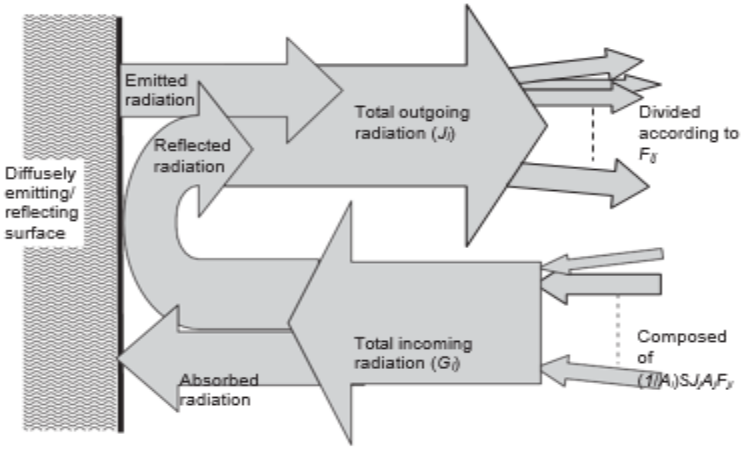

Figure 2.4. Radiation energy balance [24].

Fij is the fraction of radiation leaving surface i and reaching surface j. In this figure, Gi is the total irradiance that is incident on surface i. Ji is the radiosity of surface i. Radiosity is defined as the total radiative flux (reflected plus emitted) exiting the surface. Fij is the shape/view factor from **i** surface to j surface. Ai is the surface area for i. Solar as well as thermal wavelength can be studied independently using this approach. Thus, Figure 2.4 a system of linear equations in terms of radiosity can be solved for the net heat transfer.

For a CSP receiver, the radiation transfer can be found by knowing the concentrated solar radiation incident to the aperture and striking each surface. The aperture can be considered as a black body.

In a simple case, if the aperture is assumed to be a single surface. This aperture (at an average receiver temperature) exchanging energy with the environment, then the emitted loss (radiation) will be:

$$Q_r = \sigma A \varepsilon V_{re_{su}} (T^4{}_{re} - T^4{}_{su}) \quad (6)$$

where V_{resu} is shape/view factor between surrounding from receiver.

Similarly, reflection losses using a net absorptivity. Hence,

$$(1 - \alpha) A Q_{su} = Q_{re} \quad (7)$$

2.7 Convection losses

Wind is the main cause of convective losses. Glass cover and evacuated tubes are methods to reduce such losses.

Heat transfer coefficient is [23]:

$$Q_{conv} = hA(T_{re} - T_{su}) \quad (8)$$

2.8 Conduction losses

The material of insulation as cover for receiver are subjected to conduction losses. It is a function of temperature difference as well as of thermal resistance (material property) [19].

$$Q_{cond} = \frac{T_{re} - T_{su}}{R_{th}} \quad (9)$$

for a 1-D heat loss of thickness (L).

$$Q_{cond} = kA\frac{T_{re} - T_{su}}{L} \quad (10)$$

2.9 Linear Fresnel reflector (LFR) technology

2.10 Introduction

Historically, the usual shapes used for CSP system are [25]:

- Continuous curvature parabolic trough
- Paraboloidal disc

However, at large scale different issues were associated like:

- Expensive structure to withstand wind loadings
- Operation and maintenance

Therefore, there is a technique which can imitate large structure by aligning the smaller one with specific configuration. Thus, Linear Fresnel Reflector (LFR) arrangement, the mirrors are arranged analogous to parabolic trough technology. Similarly, parabolic dish is imitated by central receiver heliostat as shown in Figure 2.5. Presently, LFR consist of many segments of reflectors which altogether focus on receiver. The receiver is fixed at some vertical distance and run parallel to rotational axis of single axis LFR reflector.

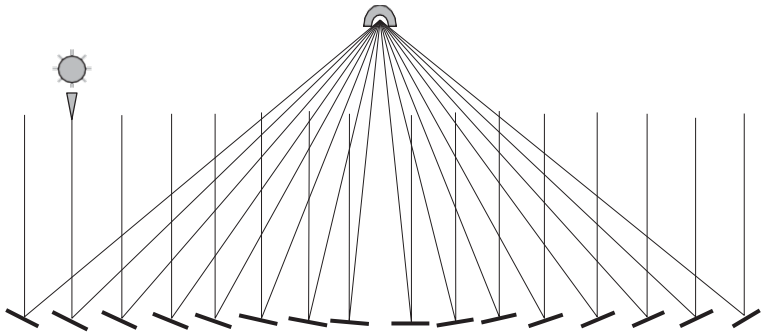

Figure 2.5. Basic linear Fresnel reflector [25].

Advantages:

- Sun tracking is single axis movement basically horizontal axis normal to receiver.
- Single degree of rotation even when the position is different according to target absorber tube.
- This leads to a unit which is a combination of large similar almost flat, lower cost glass mirror of long focal length.

In-spite of LFR approach being relatively less commercially mature than parabolic trough system, the examples may be quoted. Major commercial initiatives are:

- Areva Solar [26]
- Novatec Solar [27]
- Solar Power group [28]
- Various small Process heat initiatives commercially

2.11 Historical background

In 1818, the great French optical physicist Augustin-Jean Fresnel, revealed that many small lens components are capable to imitate the effect of large lenses. Linear Fresnel reflector solar collector systems are thus called ‘Fresnel’ reflectors. However, the famous polymath Georges-Louis Leclerc, Comte de Buffon preceded him long before. In 1746, Buffon had performed experiments using the first solar heliostat-like reflectors [29]. The system was manually tracked Figure 2.6. The system was formed out of several flat glass pieces at small angles for distant focus. Buffon demonstrated the application to ignite wood and metal melting.

Fresnel reflectors may have therefore been called as “Linear Buffon”. Buffon heliostats were two axis tracking technology. Giovanni Francia, the father of LFR and central tower system [30]. The principle was applied to larger scale solar collection in single and two axis system.

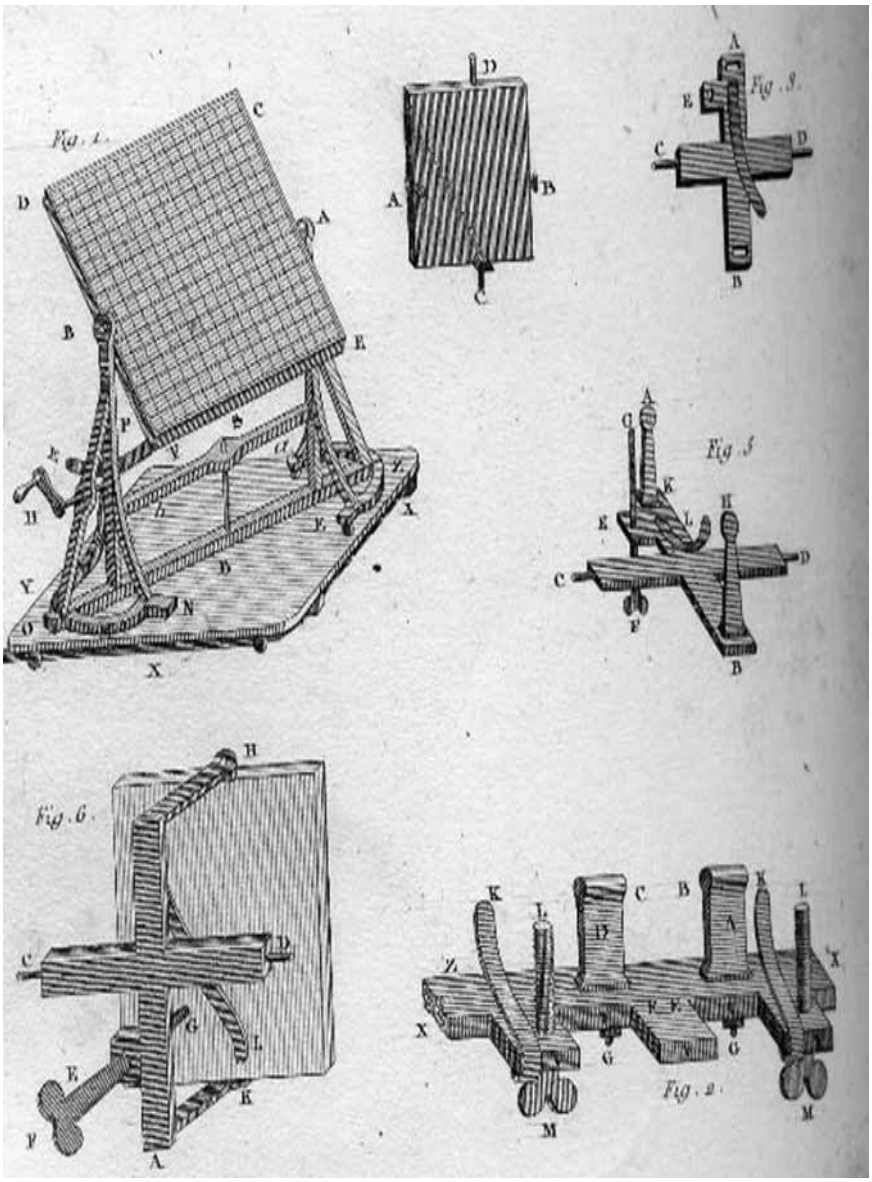

Figure 2.6. Experiments by Buffon [29].

The first prototype 1961, in Marseille, showed reach of greater temperatures using this system though the papers were insufficient in terms of efficiency as well as theory.

Figure 2.7 shows impressions of Francia drawing of linear system through Ansaldo/Cesen brochure. In 1980, future LFR plant drawings were used to develop 2008, Kimberlina plant by Ausra Inc. or Areva Solar (California).

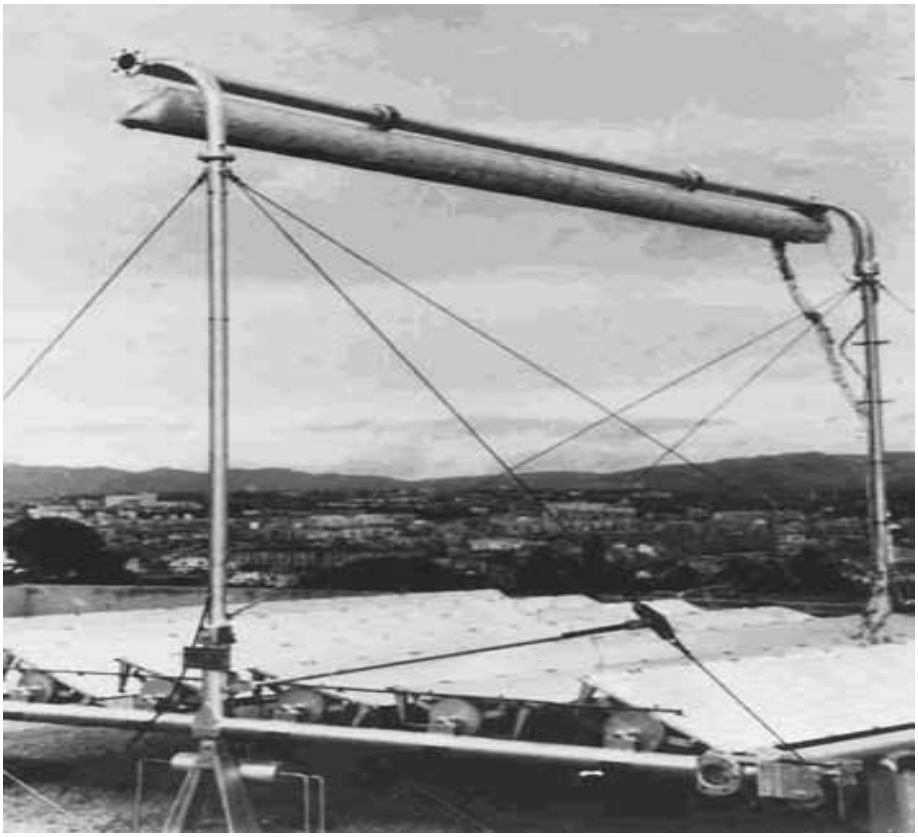

Figure 2.7. The first LFR prototype [30].

Other relevant developments with LFR system includes [31] Figure 2.8:

One designed by Suntech consisting of slightly curved mirrors, ten in number achieving a concentration ratio of 40 times. Sheldahl is known to develop the concept under government agreement however little is known further (USOTA 1978).

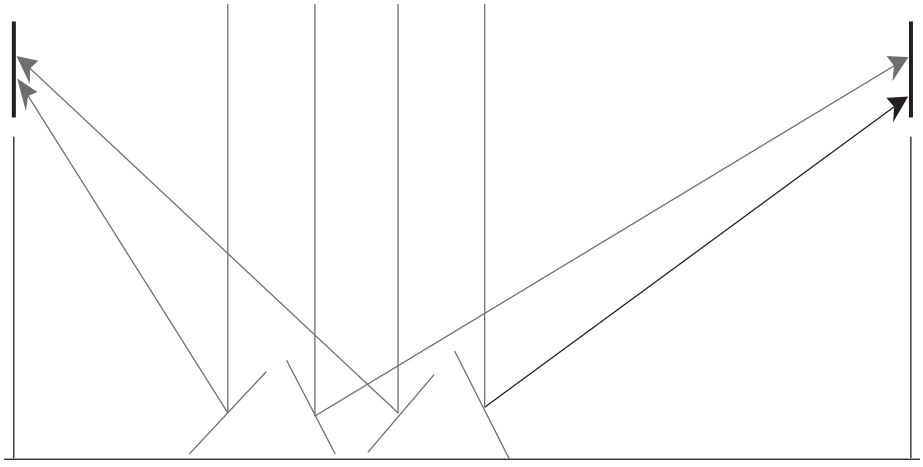

Figure 2.8. Sketch of a LFR solar plant in a desert [31].

Figure 2.9 is other design called as “Itek” evaluated trough as superior performance collectors [32]. It consisted of:

- Seven reflector mirrors
- Cylinderical glass receiver having restricted aperture
- An absorber pipe
- Insulation

A detailed specified study was made from the FMC Corporation [33]. The details are:

- A linear plant of capacity between 10 MW and 100 MW
- A mirror field for 1.68 km linear cavity
- Absorber height 61 m
- East-West axis plant
- Adjustable glass aperture cover having ability to open or close depending upon the availability of sun.

It is also during the 1970s, that secondary concentrators as well as spectrally selective absorbers undergone substantial advancement. These are helped in preventing thermal losses.

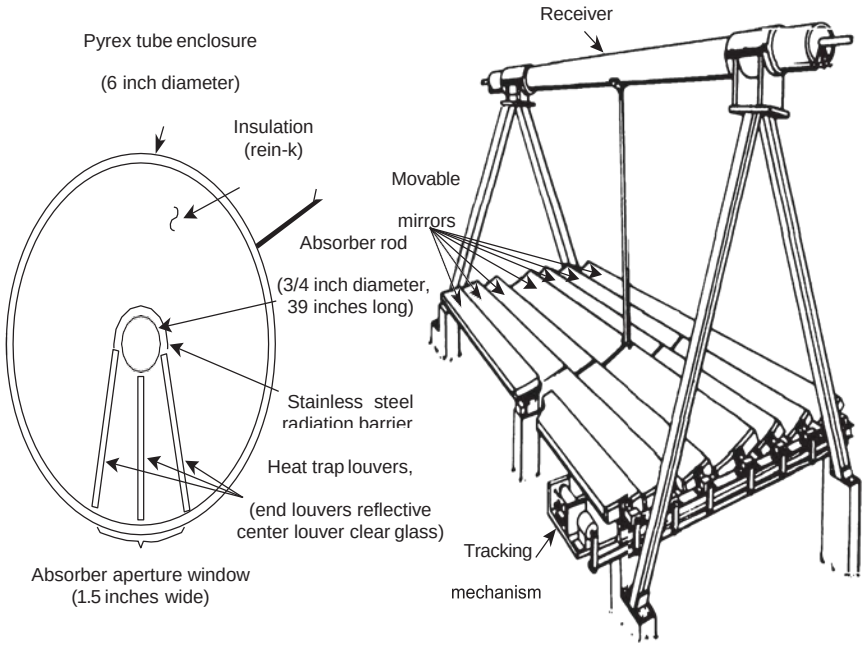

Figure 2.9. The Itek LFR [32].

After a span of decade, a new effort was made to develop an LFR with tracking ability. It was realized by Israeli company Paz during 1986. Jacob Blaustein Institute at Sede Boqer assisted the company in project [34].

Various attempts were made to increase radiation on receiver by Jeff Gordon working along with Ari Rabl and Roland Winston by using secondary concentrator. This was developed by Paz technology which include [35]:

- 150°C operation
- Secondary reflector similar to compound parabolic concentrator (Proposed with evacuated tubes)
- Mirror rows were linked together for tracking

However, issues with eccentric and non-parallel mirrors as well as linkages resulted in 2° of beam uncertainty [35]. Moreover, the array showed problems with aberration due to the movement of reflectors. This movement was along an axis parallel to the reflector optical axis, however, displaced from it. The reported performance was less than half of the value that was predicted. Figure 2.10 shows the importance of non-imaging technique for increasing concentration with the help of reflector close to receiver. This was the first LFR which made use of evacuated tubes [34].

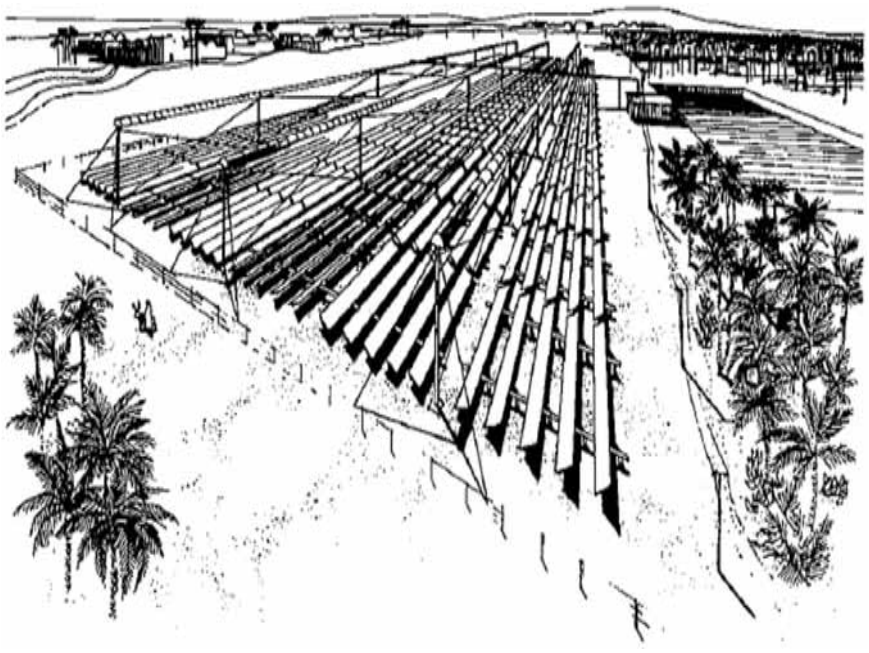

Figure 2.10. CLFR mirrors minimizing shading of mirrors [34].

Until 1993, field of reflectors used to focus on single tower. However, large scale application with wider reflector field may be extended to focus on more than two receivers placed close to each other Figure 2.10. Thus, University of Sydney, Australia developed the receiver field such that it was capable to focus on multiple receivers. This was done by changing the focal point of the reflectors to shift from on receiver to other during the day [36]. It helped dense the reflector field as well as minimized shading. The alternating receiver orientation is shown in Figure 2.11.

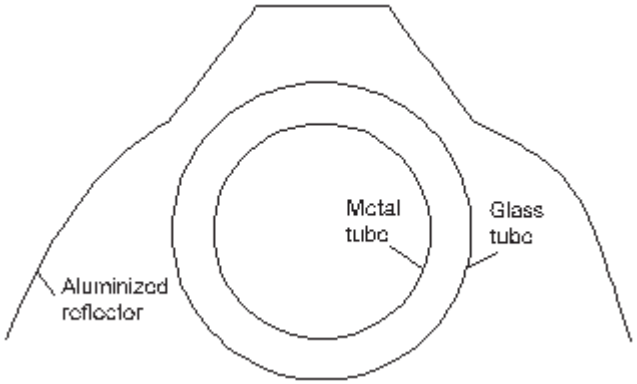

Figure 2.11. Drawing of the Paz LFR reflector [34].

This system came to be known as Compact Linear Fresnel Reflector (CLFR). As compared to trough technology, mirror area occupancy was 70% for CLFR and 33% for trough. The idea was to incorporate evacuated tube receiver however described the application of both evacuated tubes [37] and inverted cavity as in paten [38].

After development of CLFR previous works like that of Francia came into knowledge, Israeli LFR effort as well as documents and laboratory reports provided along with heliostat design reports from Paz technology [34]. The issues were:

- Degradation of secondary reflector due to greater solar flux
- Lesser efficiency (optical) due to secondary reflector (10% at that time)
- Costly parabolic trough with evacuated tubes

In order to mitigate the issues, it was decided as:

- Not to use secondary reflector
- Either Use of low cost evacuated tube array
- Or steel tube absorber with selective coating
- Inverted receiver cavity

This led to development of Areva/Ausra Solar plant. The patents and rights were given to Mills (owner of company Solsearch Pvt. Ltd.). A second patent claim with fully ganged reflector field (1997) as well as Soahart industry design of four mirror heliostat as shown in Figure 2.12 raised the interest in Solar field after climate meeting of Kyoto. In 1999, Austa Energy with Solsearch agreed to develop 4MW CLFR plant (grant from Australian Greenhouse Renewable Energy

Figure 2.12. Solahart comparing evacuated and non-evacuated absorbers [39].

Showcase Scheme). This project was also supplied with coal fired existing plant Stanwell and conceptual work was demonstrated [39]. These are now called as “Solar booster plants”.

Figure 2.13. Ray trace CLFR with multiple receivers [40].

During 1999, comparison studies were made by the Austa/Solsearch project group while designing new receiver cavity. It was found that [40]:

- Black coated steel tubes were compared with evacuated tube absorbers
- Single vacuum absorber could not be used as absorber (small capacity)
- Larger optical losses with multiple evacuated tubes

Hence, improved design as shown in Figure 2.13 was developed with inverted trapezoidal receiver cavity with flow modelling [41]. A backbone and rib structured heliostat was also developed be Solahart as shown in Figure 2.14.

The technology that got bankrupted (Luz Technology assets) was purchased by Belgian investors in 1993 (trough and evacuated tube technology) [42]. Two companies (Solel Israel and Solel Europe) were created (confidential agreement with University of Sydney) to visualize the concept:

- Nylon gears to run flat mirrors
- Torque tubes
- Single tube single end steam receiver tubes with internal water feed mechanism
- Non-imaging CPC reflector (secondary)
- vacuum receivers

Figure 2.14. Prototype backbone and rib heliostat [42].

Solel Europe became insolvent and project was discontinued 1995. Further, University of Sydney developed a revolutionary prototype [43]:

- Evacuated tube
- Double cermet
- Solar selective coatings

Solarmundo company in 1998 developed [44] 2400 m^2 which was the largest LFR array in reflector field without mirror flipping by 2001 as shown in Figure 2.15 [45].

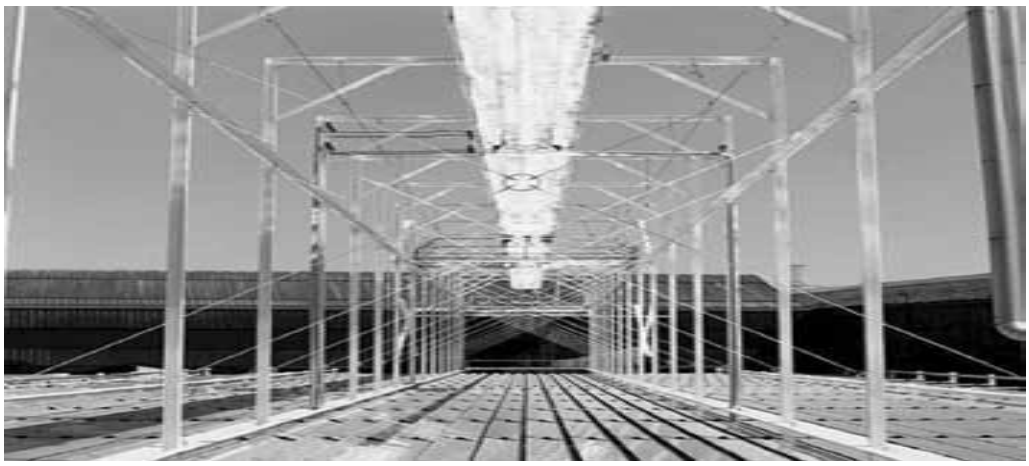

Figure 2.15. The Solarmundo prototype [44].

2.12 Areva Solar (formerly Ausra, Solar Heat and Power)

In late 2001,the planned [46] array as shown in Figure 2.16 under company name Solar Heat and Power (SHP), Sydney [47].

Figure 2.16. First sketch of the SHP [47].

Following the Solsearch design, the new system was as follows [48]:

- Avoided secondary receivers to minimize not only optical losses but also surface degradation of reflectors
- Low cost drive hoops as tracking system was chosen
- Inverted trapezoidal cavity with connected absorber tubes Figure 2.17.
- New SHP design which used separate absorber tubes for thermal expansion

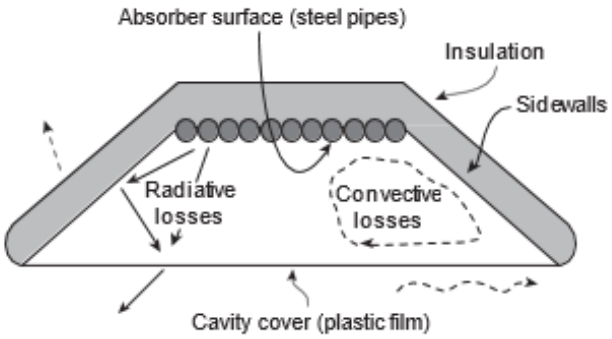

Figure 2.17. trapezoidal cavity with a plastic cover [48].

In 2003, as a coal booster plant at Liddell Power Plant this technology was concluded to develop with an agreement of Macquarie Generation in New South Wales. By 2004, the developed SHP details are [49]:

- Not connected to main power block
- 61m long, 1340 m^2 LFR prototype
- 1 MW power station Figure 2.18

Figure 2.18. Stage 1 of the Liddell array [49].

- Operating parameters with respect to preheater (280°C and 80 bar)
- Figure 2.19 shows layout of SHP

By 2004, future plans were developed [46] with

- 16 parallel pipes, 25 in number, each 60 m long (SS 304 material)
- Mounting side by side to allow for thermal expansion
- Absorber width of 575 mm
- Pipes were connected to achieve a flow path of 240 m
- Centre pipe returned superheated steam as water is the feed
- Non-selective coating for pipes (black)
- Anti-reflective coating for inverted cavity

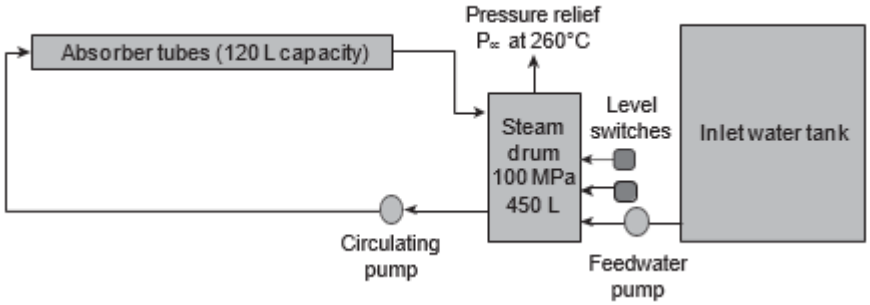

Figure 2.19. Schematic prototype at Liddell [48].

LFR technology could be used for [50], [51]:

- Operating temperature 300°C
- Low pressure nuclear turbine incorporation as low cost power generation
- It can compete trough technology [52]
- Since only air stable coatings (black chrome) were available hence operating temperature was that of preheater temperature

Liddell Project (2006) stage 2 includes:

- 20,000 m^2 5 MW power plant
- Connected to main power block
- Improved collector design Figure 2.20
- Mirrors increased reflectivity from 84% to 92.5%

- Reflector width reached 2.25 m from 1.82 m
- Length from 12.2 m to 12.9 m
- Absorbers from 12 to 10 in number
- Tower and absorber dimensions unchanged

Figure 2.20. Stage 2 of the Liddell array [46].

In 2008, Kimberlina [53] in Bakersfield (California) Figure 2.21 built:

- A-frame tower (similar to 1970 “itek” tower)
- 384 m line, 5 MW biomass steam turbine
- 25,988 m^2, 30 reflectors rows with 24 modules per line
- Each mirror module has 36.1 m^2 of area, five reflector panels 2.25 m wide for 16 m.

Figure 2.21. The three-line Kimberlina array [53]**.**

By 2010, utility CS Queensland secured [50]:

- 44 MW 18-line steam booster plant
- Operating temperature 330°C
- Technology was selected for 250 MW

Similar project (250 MW) to be built in India by Areva Solar. Areva Solar also started studies for 150 MW CLFR (free-standing) plant [54] to be installed in Fresno, California.

Areva Solar has tested a fourth line Figure 2.22 newer technology called SSG4 [55]:

Figure 2.22. The fourth line at Kimberlina superheating line at 400°C [55].

- Pressure of 92 bar
- 13 mirror line configuration (unlike previous ten)
- Superheated steam receiver (unlike previous saturated steam line)
- 11,261 m^2 area for 13 reflector rows (24 modules per line)
- Performance test for 400°C (Black and Veitch engineers)
- Light out capacity to deliver 18 min of superheated steam (thermal inertia)

Areva is developing a 482°C, 165 bar operation (Areva, 2012) plant. It consists of 13 reflector line with a maximum absorber pipe wall of 482°C. In its version 2.0 0 (under development), it is possible for maximum steam greater than 500°C.

2.13 Solar Power Group (formerly Solarmundo, Solel Europe)

The Solel Europe with Belgian investors found Solarmundo 1990s [28]. The design was an LFR using a non-imaging receiver secondary reflector for use with a custom-built non-evacuated absorber tube, a similar concept to the earlier Paz receiver design.

The Count de Lalaing founded Solar Power Group (SPG) for LFR work [52], [56]–[58]. This prototype used the resources of PSE (German research institute) to counter

- the issues of optical reflector design
- Selective coating durability at higher temperatures
- Secondary mirror stability

The Plataforma Solar de Almería (PSA) 2007 in Spain (Figure 2.23, Figure 2.24) improved FRESDEMO pilot collector. The DLR's Institute of Technical Thermodynamics investigated the thermal behavior and losses as well as thermal efficiency with varying receiver temperatures. The FRESDEMO re-optimized design:

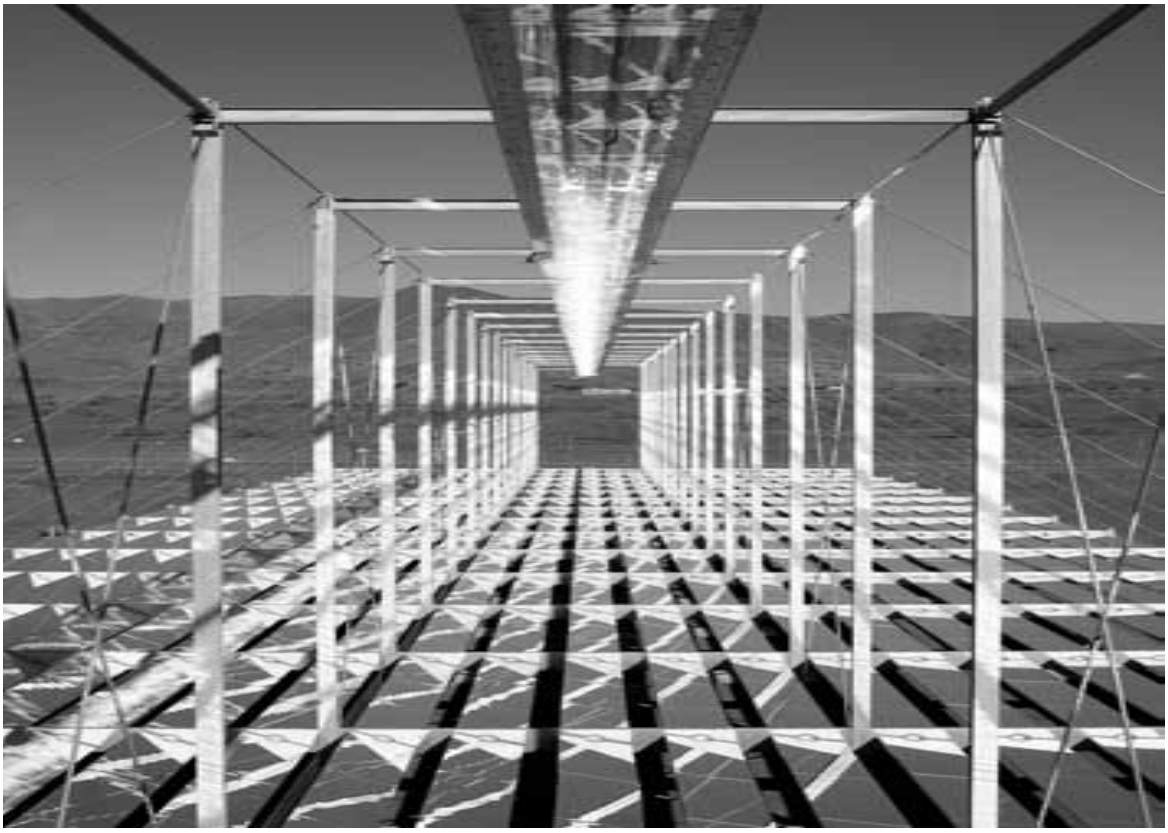

Figure 2.23. The FRESDEMO SPG prototype [56]**.**

- 100 m length, 21 m wide including 15 m of cumulative mirror surface width
- The absorber pipe of 14 cm outer diameter and 12.5 cm inner diameter
- 15 m^2 of reflector per linear meter of absorber tube
- The geometrical concentration is 34, about 20% higher than troughs
- Slightly curved mirrors

The FRESDEMO collector operation can be modified to select any of the three modes [56], [59]:

Figure 2.24. Public showing of the FRESDEMO prototype [59].

- preheating (absorber fed with preheated water or cold water)
- evaporation (absorber fed with saturated steam and preheated water)
- superheating (absorber fed with superheated or saturated steam only).

The optical efficiency reduced from 63% to 53% which restored after cleaning [59]. The FRESDEMO design issues

- loss of 850 W of thermal energy per meter of receiver length at 300°C
- The thermal loss of 57 W/m^2 of field reflector

This loss was higher than Novatec Solar and Industrial Solar (secondary reflector design). This is likely because:

- Novatec based the design for higher optical concentration on receiver
- Industrial Solar applied low loss evacuated tubes

FRESDEMO new improved model in 2008:

- Operating temperature 450°C
- In-line superheater for trough direct steam generator (SPG, 2008)
- Highest temperature (greater than most of parabolic trough technology)

The technical aims of SPG (with the Fraunhofer Institut für Solare Energiesysteme (ISE) and the German Aerospace Center (DLR)) as stated in [56] were:

- 70 mm evacuated tube
- Reduce thermal loss and improve overall efficiency (even on considering 10% optical loss)
- Smaller evacuated tubes led to 80% of PTC cost [4], [60] (current model 53% of PTC)

In 2010, SPG in Mejillones with GDF Suez to construct:

- 5 MW add-on onto a coal-fired power plant.

2.14 Industrial Solar (formerly Mirroxx, PSE)

PSE AG is a spin- off of Fraunhofer ISE the solar technology company of solar research institute in Freiburg. PSE 2005 developed a small LFR called FL-11 using [12]:

- A single 70 mm diameter Schott evacuated tube receiver
- for the process heat market
- employs an A-frame support (similar to “Itek” collector)
- 16 bar water circuit, 200°C process heat operation
- 4 m long, 8 m wide and 11 primary mirror rows flat white glass mirrors (slightly curved elastically)
- Polished aluminum secondary reflector

A second prototype in Bergamo, Itlay 2006:

- an aperture area of 132 m^2
- 66 kW to power an ammonia-water absorption chiller

In 2007, Escuela Técnica Superior de Ingenieros (ESI) rooftop installation [61]:

- Fresnel process heat collector
- 352 m^2 aperture area
- 176 kW (Figure 2.25)
- 64 m collector length (16 × 4 m long modules)
- 5.5 m^2 of reflector per lineal meter of receiver
- powers a double effect H_2O/LiBr absorption chiller (capacity of 174 kW)
- a coefficient of performance (COP) of 1.3

Figure 2.26. The third Industrial Solar project operating temperature 180°C [61].

In 2008, fourth project, a solar cooling system (NH_3/H_2O chiller) was developed in Winery. (Figure 2.26) the largest LFR in Doha Qatar [12], [61]:

Figure 2.25. Industrial Solar Fresnel collector field in Doha absorption chiller [12].

- to power an absorption chiller (500-seat football stadium) (December 2010 issue of Renewable Energy World)
- single-axis tracking flat-plate mirrors
- Schott PTR® evacuated tube receiver
- 16 bar at 200°C water as HTF
- Collector aperture area 1,400 m^2
- 700 kW thermal output
- direct normal irradiation (DNI) of 62% efficiency

2.15 Novatec Solar (formerly Novatec-Biosol, Turmburg Anlagenbau)

In 2005, a new LFR Figure 2.27 company was formed, called Turmburg developing [12]:

- a CPC cavity receiver (resembling the SPG design)
- 70 mm receiver (like the PSE design)

- design tower (similar to the small ‘V’ support used in the V1.1 SHP CLFR)
- revolutionized reflector construction (lightweight, mass production, no motors for rotation)

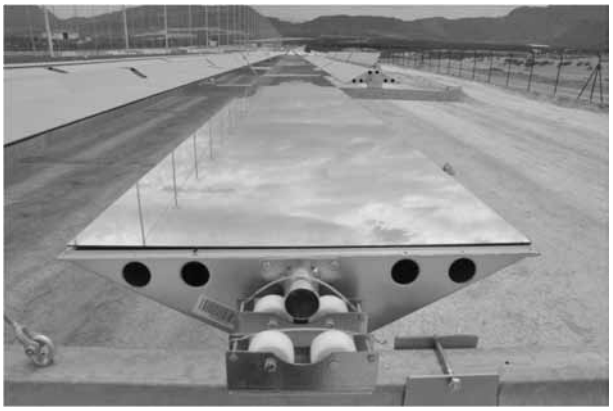

Figure 2.27. Novatec reflector polymer support bearings. [12].

In late 2006, a prototype plant in Spain [2] Figure 2.28 and Figure 2.29:

- 270°C operation, 128 reflectors (16 reflector lines)
- The basic solar boiler module was called Nova-1
- receiver height of 6.2 m from ground
- mirror hub height 1.2 m above the ground

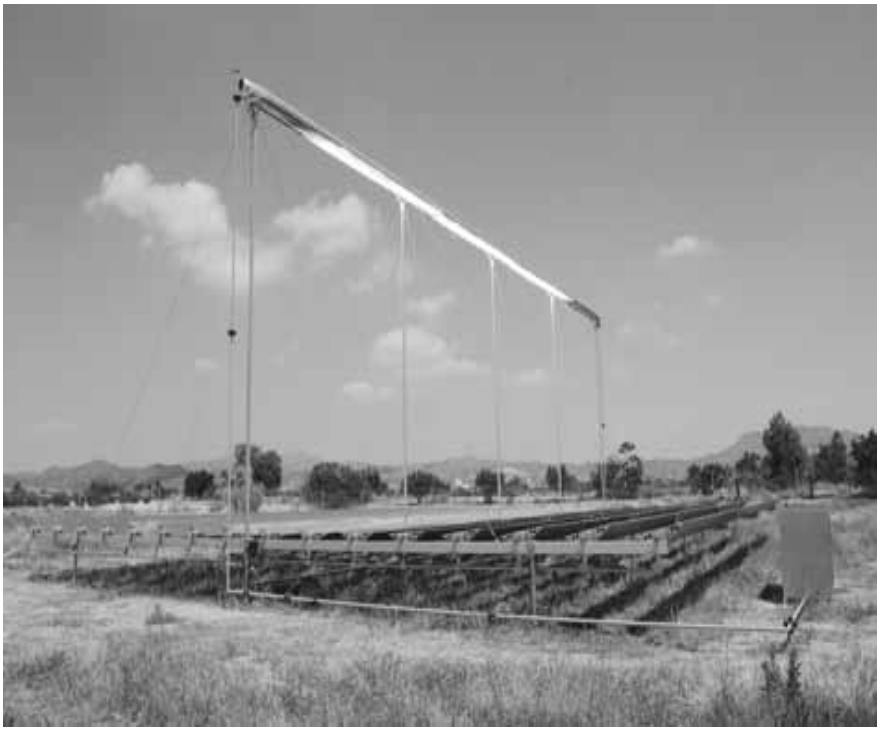

Figure 2.28. The 2005 Novatec [2].

Figure 2.29. Novatec dry cleaning robots [2].

The plant PE-1, located in Calasparra (Spain) Figure 2.30:

- a capacity of 1.4 MW
- optical efficiency of 67%
- The two parallel collector rows
- a length of 806.4 m
- steam–water mixture at up to 55 bar (270°C) Figure 2.31
- steam and water phases separation in steam drum (steam to turbine and water recirculated)

Figure 2.30. PE-1 1.4 MW powerplant [12].

One year later, it constructed PE-2 with:

- 30 MW, 302,000 m^2 of collector area
- temperature conditions: 100°C inlet; 270°C outflow and 40°C ambient
- 246.2 kW per module
- 900 W/m^2 direct normal radiation (DNI)

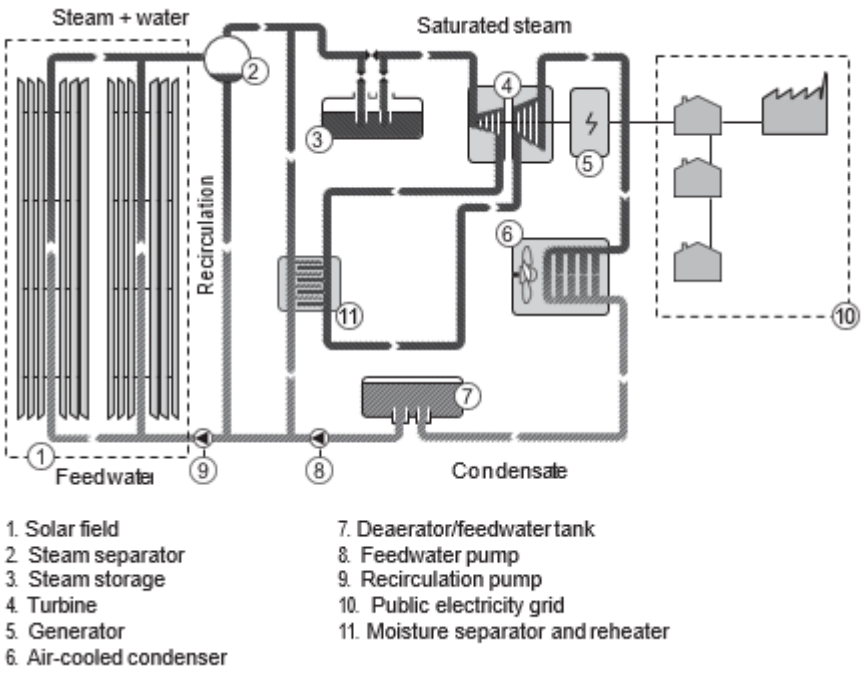

Figure 2.31. PE-1 1.4 MWe powerplant schematic [12].

2.16 Absorber materials for solar thermal receivers

Two basic collector types of line focusing systems Figure 2.32 are [62]:

- the parabolic trough collector (PTC), (complete parabolic mirror)
- the linear Fresnel collector (LFC) (the parabolic shape is split up as per Fresnel principle)

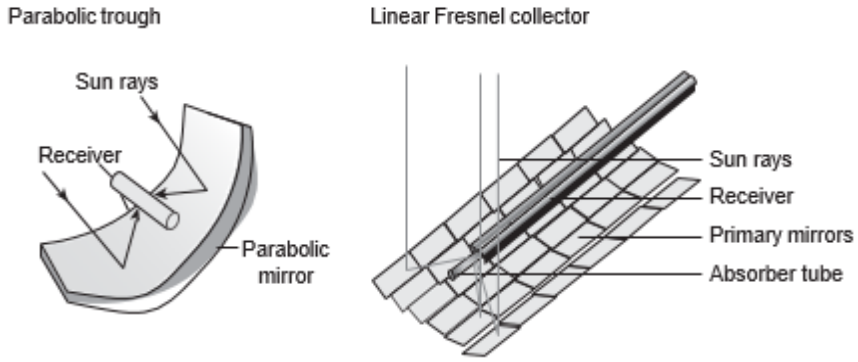

Figure 2.32. Parabolic trough (left) and linear Fresnel collectors (right) [62]**.**

Absorber tubes (blackened) carry HTF to convert solar flux into sensible heat. The surface of absorber pipe should have [63]:

- a very low reflectivity

- high absorptivity.

2.16.1 Ideal selective absorber

An ideal selective absorber surface is black (i.e., completely absorbing). In the solar wavelength range (0.3 μm to 2.5 μm), to reduce the thermal losses it should have low emissivity (for emitted wavelength). Absorber surfaces are based on principle [64], [65]:

- the absorptivity equal to emissivity i.e. the fraction of incident radiation it absorbs equals the amount an ideal black body would emit
- all the incident radiations must either be reflected, absorbed or transmitted. The sum of reflectivity, transmissivity and absorptivity must be unity.

The primary idea of a selective surface is that emitted wavelengths from receiver are different than solar spectrum. As a result, the ideal reflectance is a step function. High absorptivity in solar wavelength and low emissivity in thermal radiation [66]–[68].

2.16.2 Types of selective absorbers

It can be categorized as:

- Homogeneous material.
  - (a) intrinsic
  - (b) semiconductor–metal tandems
- Non-homogeneous material.
  - (a) multilayer absorbers
  - (d) multi-dielectric composite coatings
  - (e) textured surfaces
  - (f) selectively solar-transmitting coating

Intrinsic absorber coatings consist of a material having selective inherent properties that produce the desired spectral selectivity. Semiconductor-metal tandems have metal layer and have low thermal emittance. It can absorb short wavelength radiation (above semiconductor bandgap). Multilayer absorbers use multiple reflections between layers. Metal-dielectric composites (cermets) use small metal particles in a ceramic or di-electric host material. Textured surfaces have needle-like, dendritic, or porous microstructure. It can lead to high solar absorptance by multiple reflections. Selectively solar-transmitting coatings are used on low-temperature applications (on a blackbody- like absorber) Figure 2.33 (a)– (f). Table 2.1 and Table 2.2 provides a review [65], [69]–[72].

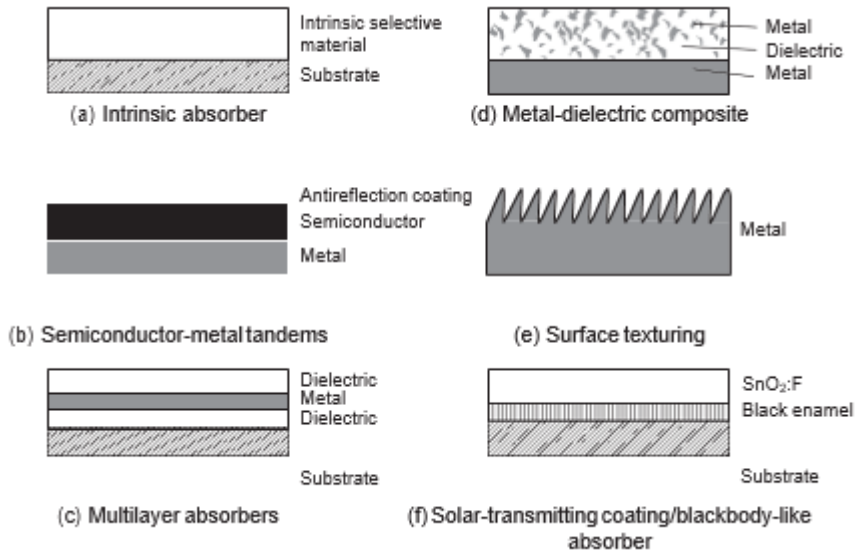

Figure 2.33. (a) Schematic of coatings and surface treatments [65].

Table 2.1. Mid-temperature selective surface [65].

Rank	Material	Substrate	Fabrication	Absorptance	Emittance ε (100°C)	Stability (°C) vacuum	Stability (°C) air	Commercial product
2	TSSS[a]	Al	Paint	0.92	<0.015		<135	Solariselect
2	PbS	Al	Evaporation Pyrolysis	0.93–0.99	0.21–0.10		200	
2	NiCrOx	SS[b]	Sputtering	0.8	0.14		<200	
		Cu/Polyamid		0.92–0.93	0.06		<200	
2	Colored SS	SS	Chemical conv.	0.62–0.93	0.1		<200	SEL, INCO
	Black nickel							
2	NiS-ZnS	Ni coated	Electrodepositi	0.88–0.96	0.03–0.10		<200	Maxorb
3	Ni-Sn	Cu	Electrodepositi Sol-gel	0.92–0.98	0.08–0.25		300	Black Crystal
	Graphitic films							
3	a-C:H/Cr	Cu	MF-pulsed	0.92	0.025		250	
	a-C:H	Al	PVD/PECVD	0.876	0.061		250	
3	Ge *in*	Cu or SS	Paint	0.91	0.7		300	
	Si *binder*			0.83	0.7			
	PbS			0.96	0.7			
3	Ag dielectric	Al	Biomimetic				300	
3	*Black copper*	Cu	Electrodepositi	0.97–0.98	0.02	370	250	
	BlCu-Cu2O:Cu							
3	*Black chrome*	Ni-Cu	Electrodepositi	0.97	0.09	400	350	MIT
	Cr-Cr2O3	Cu steel						ChromeCoat
3	Mo/ Cr2O3			0.95	<0.30		425	Energie

								Solaire
3	TiN_xO_y	Cu	ARE	0.92	0.06	400		Thermomax
2	CuFeMnO4/sil	Glass,Si	Sol-gel	0.6	<0.29–0.39			
1	Cr,Fe,Mo,SS,T	Bulk Cu	DC reactive	0.76–0.82	0.02–0.3		400	
	Ti,W silicides	Sputtered Cu	Sputtering	0.81–0.86			250	
1	Cr,Fe,Mo,SS,T	Bulk Cu	DC reactive	0.76–0.81	0.02		400	
	Ti, W	Sputtered Cu	Sputtering	0.81–0.86	0.035–0.06		250	
3	$Ni-NiO_X$	Al	Reactive	0.096	0.10		300	Sunstrip
3	Ni pigmented	Al	Anodization	0.85–0.97	0.08–0.21		300–400	Tekno Term

Table 2.2. High-temperature selective surfaces [65].

Rank	Material	Fabrication	Absorptance	Emittance ε (100°C)	Stabilit y(°C) vacuum	Stability (°C) air	Commercial product
2	$Ni-Al_2O_3/SiO_2AR$	RF sputtering	0.94	0.07	500	350–400	
2	$Co-Al_2O_3$		0.94	0.04			
3	$Mo-Al_2O_3$	RF sputtering	0.96	0.16 (350)	350–500		Solel
1	$W-Al_2O_3$	RF sputtering	0.97–0.98	0.1–0.07			Solel
	$W-Al_2O_3$	CVD	0.85	(400)	500		
1	$Pt-Al_2O_3$	RF sputtering				600	
1	$Al_2O_3-Pt-Al_2O_3$		0.90–0.98	0.08		600	
	Double				500		
1	$Mo-Al_2O_3$	DC-sputtering	0.96	0.06 (350)	350–500		TurboSun
2	SS-AlN		0.95	0.10 (350)	500		
3	Mo-AlN		0.92–0.94	0.08–0.10	500		
1	W-AlN						
	Quasicrystals						
1	Multilayer		0.90	0.025	500	400	
1	Cermet		0.86–0.92	0.031–0.05	550		
3	$Si_3N_4/Si-Ge/Ag$	CVD	0.890	0.0389 (300) 0.0545 (500)		650 (He)	
1	$Ni:SiO_2$	Reactive	0.90–0.96	0.03–0.14		4	
	Cr:SiO	DC				0	
3	$Al-AlN_X-AlN$	Reactive DC	0.97	0.10	500		
2	CuO	Electroplating	0.91	0.18		>400	
1	$Ag/CuO/Rh_2O_3/CeO_2//$	Organo-	0.9	0.1	700	500	
1	$CeO_2//Ag/Pt/CuO/Rh/$		0.86–0.88	0.1	775	550	
1	$CeO_2//CuO/Co$			0.88–0.92	0.06–0.12	700	
	Black cobalt						
1	Co_3O_4/Co			0.96–	0.71–0.017		
3	$Ni-Co_3O_4/Co$			0.95	0.10		
	Black moly		CVD	0.94	0.30 (500)	500	
1	$Mo-MoO_2$						
	Black tungsten		CVD	0.83	0.15	800	
1	$W-WO_X$						
1	Au/TiO_2	SS	Sol-gel	0.85	0.01(400)	>500	
3	Au/MgO	Mo/SS	RF sputtering	0.90–	0.04–0.1		
3	ZrC_xN	Al		0.85	0.074 (325)	600	
3	$Al_2O_3/ZrC_xN_y/Ag$			0.91	0.05 (325)	700	
1	$ZrO_X/ZrC_X/Zr$	SS		0.90	0.05 (20)	700	
3	TiN	Cu,Al	DC reactive	0.80	0.14–0.40		

1	$Ti_{1-x}Al_xN$		sputtering				750
3	M_bO_c□M'Fe_2O_4	Ni-Mo alloy	Painting Arc plasma	>0.90	>0.45		
3	VB_2, NB_2, TaB_2, TiB_2,ZrB_2,LaB_6, WSi_2,$TiSi_2$	Glass	DC-reactive sputtering	0.99	0.95–0.97	2300–3040 (MP)	
1	Si_3N_4 AR-ZrB_2	ZrB_2	CVD	0.88–	0.08 to 0.10		
3	Masterbeads®			0.93			
2	C-Textured Cu	Cu		0.9	0.04(20)	400	
2	Textured Ni	Ni		0.92	0.09±0.02		
1	Textured SS			0.93	0.22±0.02	>440	
3	Textured Cr	SS		0.80–	0.10–0.30		
1	W whiskers	Cr		0.98	>0.26	550	
1	Mo, Rh, Pt, W, HfC, Au						
1	NiO_x, CoO_x	800					

2.17 Receivers for linearly concentrating collectors

2.17.1 Vacuum tube receivers for parabolic trough power stations

Linear Fresnel unit's receiver with absorber tubes are shown in Figure 2.34. Vacuum tube receivers [73]. The absorber tube is borosilicate and coating is stable for 400°C operation [73], [74].

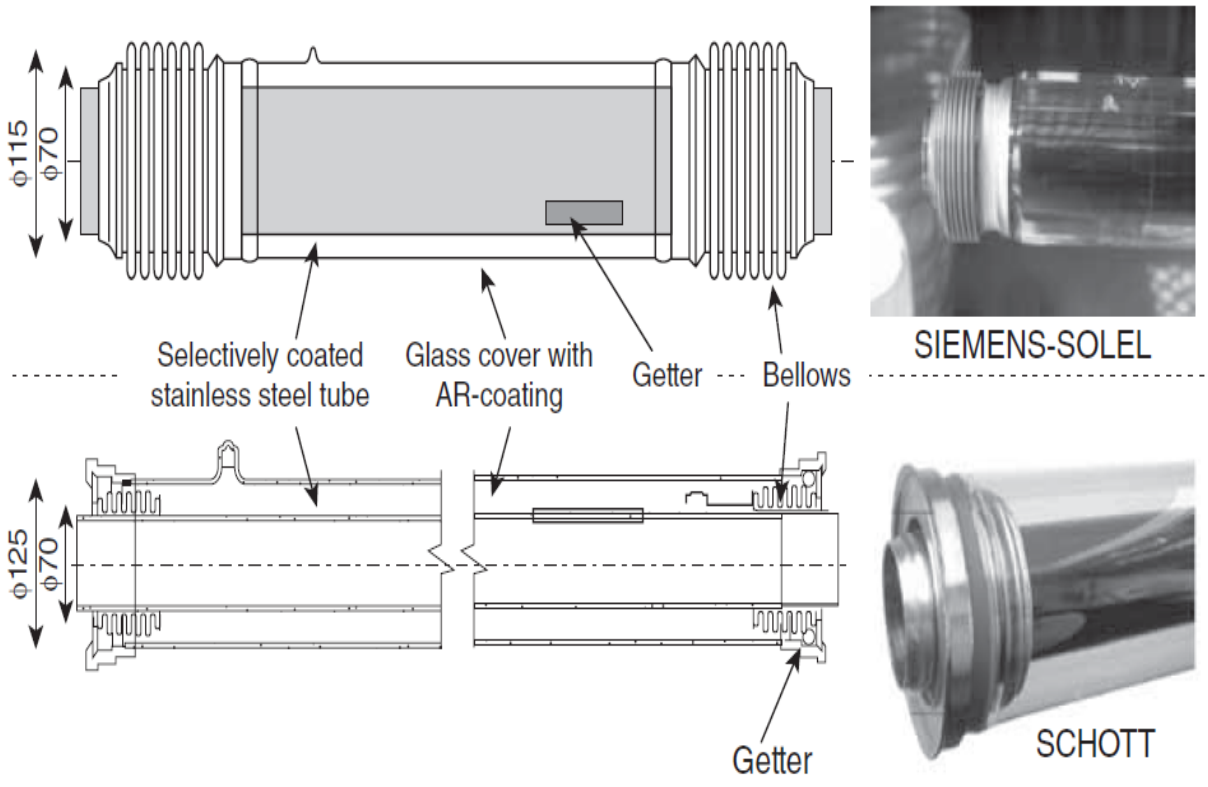

Figure 2.34. Vacuum tube receivers [73].

The tube is provided with Al_2O_3 diffusion barrier. The Mo/Al_2O_3-cermet, Mo-IR-mirror and the SiO_2 AR layer is deposited on the tube [75], [76].

ENEA developed a DC (direct current) sputtered absorber system. It consists of a 500 nm thick W or ZrN-IR-mirror. A cermet of ZrN_x, TiN_x or HfN_x in AlN. The AR layer is made from AlN or Al_2O_3. The coating is stable for 580°C in vacuum[77], [78].

2.17.2 Air stable receivers

It used stainless steel tubes. Other materials Cr, Mo, Ni, and Ta has been investigated as IR-mirrors Figure 2.35. One problem for these materials is fast oxidation in air. In case of Silver (Ag), the main degradation mechanism is Ag_2S formation on reacting with H_2S in air. However, polished stainless steel, a CrO_x cermet with a SiO_x-AR layer was stable at 500°C [71].

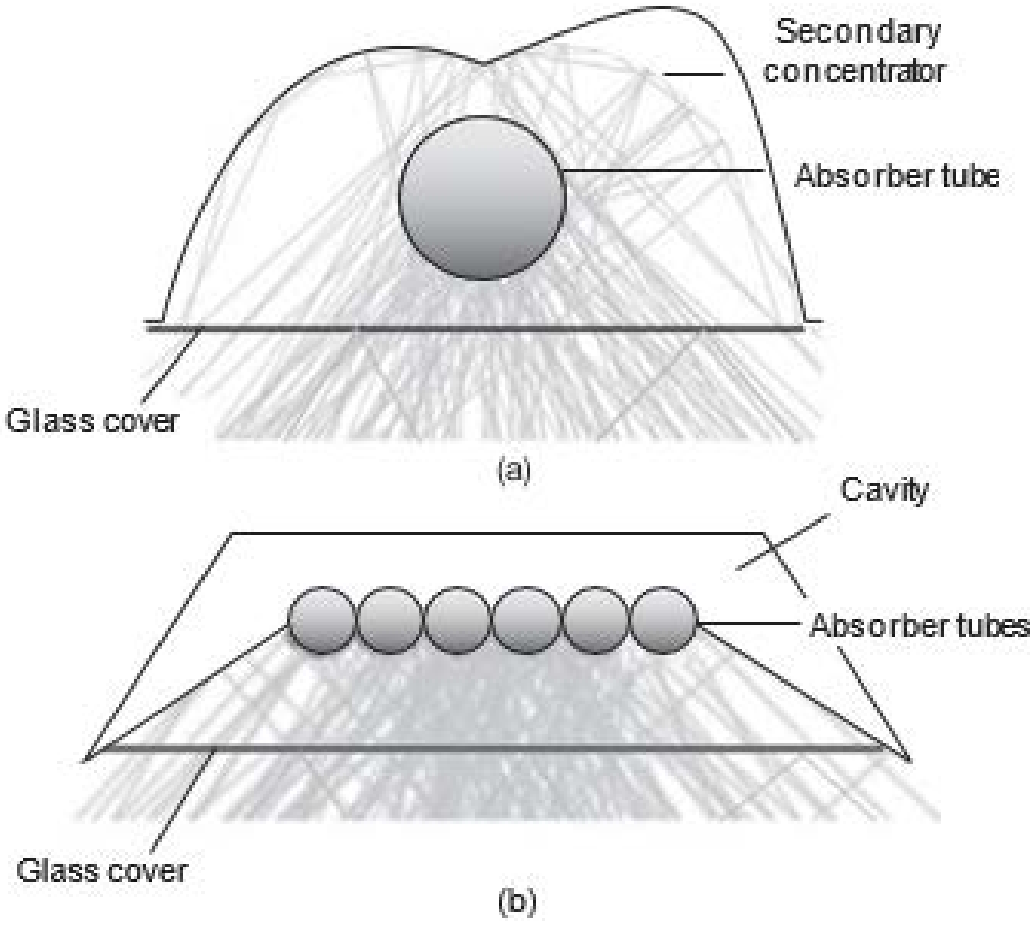

Figure 2.35. Receiver (a) single tube (b) multi-tube [74].

CHAPTER-III

3 Literature Review

David R Mills et al 1997 [6] presented a commissioned report regarding new Solar Technology called as Compact Linear Fresnel Reflector (CLFR). The study reports performance as well as cost for the large scale application of solar thermal plant. Among Parabolic Dish, Solel trough and photovoltaic plant the comparison concludes CLFR as the lowest cost option for solar electricity.

D.R. Mills et al 2000 [79] studies were performed for Stage 1 CLFR plant at Lidell Power Station. The study found a considerable matching between modelling predictions and measurement results. A peak thermal output of 100 MW during summer can be achieved. In winter conditions, steam is generated with 0.95 dryness fraction (80 bar). Direct steam generation in trough technology is far complex than in CLFR.

D J Reynolds et. al 2002 [80] proposed innovative direct Steam Generation (DSG) collector based on CLFR technology. Heat loss correlations were obtained. Further, a hydrodynamic model was generated to predict effect of tube-diameter on pressure drop as well as mass flow rate.

John D Pye et. al 2003 [48] numerically studied CLFR trapezoidal cavity wih varying cavity depth, width, absorber temperature, convective coefficient as well as ambient temperature. Correlations for Grashof as well as Nusselt number were obtained neglecting the scattering of radiation and unsteady effects.

D.J. Reynolds et. al 2004 [41] investigated heat loss from CLFR plant having absorber tubes behind flat absorber plate. Flow pattern visualization through experimental technique in agreement with computational work. The developed model could be applied to various optimization and control methods for CLFR type solar collector.

Soteris A Kalogirou et. al 2004 [81] had done a review survey for various solar thermal collectors. The available technology is analyzed for vast range of applications. Various analysis for optical, thermodynamic and thermal efficiency were described as in Table 3.1. Since these systems provide benefit for applications like desalination, thermal power system, solar furnace, chemical applications etc. hence should be used as possible. Data for concentration is provided in the survey for various collectors.

Table 3.1. Categorization of solar collectors [81].

Motion	Collector type	Absorber type	Concentration ratio	Indicative temperature range (°C)
Stationary	Flat plate collector (FPC)	Flat	1	30-80
	Evacuated tube collector (ETC)	Flat	1	50-200
	Compound parabolic collector (CPC)	Tubular	1-5	60-240
Single-axis tracking			5-15	60-300
	Linear Fresnel reflector (LFR)	Tubular	10-40	60-250
	Parabolic trough collector (PTC)	Tubular	15-45	60-300
	Cylindrical trough collector (CTC)	Tubular	10-50	60-300
Two-axis tracking	Parabolic dish reflector (PDR)	Point	100-1000	100-500
	Heliostat field collector (HFC)	Point	100-1500	150-2000

D Mills et. al 2004 [82] reviewed various advanced solar thermal technologies i.e. single-axis, two-axis tracking and low temperature application etc. CLFR is described as the potential technology competing single-axis tracking technology. A cost of US $0.06 per kWh for Rockhampton CLFR and US $1.0655 in Solarmundo Spain is stated from solar electricity.

D.R. Mills et. al 2006 [83] innovated CLFR previous design and used two alternative receivers which allowed for more densely packed array of mirrors. This was developed in the light of trough technology that reached its design limitations of absorber surface coating and large scale collector configuration needed. Various configurations of absorber orientation, secondary reflector, reflector field configurations etc. were investigated to that of basic CLFR version. Development of ray trace and thermal models for simulation studies was concluded as the need of the hour.

C.J. Dey et. al 2006 [84] carried out study for DSG based on CLFR concept with absorber plate. The main aim was to increase heat interactions between steam pipe and absorber surface. Moreover, uniform absorber plate temperature was ensured to reduce degradation. Using finite analysis temperature difference of less than 20 K can be achieved for optimum values of plate thickness as well as pipe separation distance.

John D Pye et. al 2006 [85] obtained an agreement with modelling data and experimental values for pressure drop analysis in DSG CLFR plant piping system. Extended modelling work was framed to include bends, valves, connecting pipe work with application of updated heat loss as well as pressure drop correlations.

John D Pye et. al 2007 [86] presented transient model for DSG receiver of a CLFR plant. The Friedel pressure drop as well as homogeneous flow assumptions used for the two phase flow in ASCEND modelling software. Moreover, CLFR prototype is investigated for pressure drop and flow rate instabilities which could be corrected using orifices. It is concluded that increasing the quality of exit steam increase efficiency slightly as well as the chances for undesirable superheated steam.

C.E. Kennedy et. al 2008 [87] provided information regarding advanced solar selective coating besides various solar data for different states. It concluded that IBAD Al_2O_3 mirror have a potential to meet CSP needs.

Panna Lal Singh et. al 2010 [88] investigated an extent of variables for trapezoidal cavity used in linear Fresnel applications water heating (60-95 °C). There was an effect of thermal coating and concentration on thermal efficiency could be seen. 10 % more efficiency obtained for selective coated surface and 2-8% higher for round pipe absorber as in Table 3.2. Thermal efficiency from experimental data as well as correlated data was within range of ±12%. Moreover, Hytherm-500 was recommended for heat transfer fluid (280 °C) with superior heat transfer properties.

Table 3.2. Effect of concentration ratios [88].

Concentration ratio of the collector	Thermal efficiency of the Fresnel reflecting collector (η) (%)			
	Rectangular pipe absorber		Round pipe absorber	
	Ordinary black painted	Selective surface coating	Ordinary black painted	Selective surface coated
19.8	15.6-35.8	25.0-43.2	16.0-38.1	25.7-45.7
17.6	18.7-39.8	28.4-47.5	20.7-41.3	29.0-50.8
1.2	23.4-45.0	30.4-54.6	24.3-46.5	35.0-58.7
12.4	26.9-50.6	34.7-57.2	28.7-52.9	40.2-64.9
9.4	28.3-54.3	38.3-63.0	30.5-59.6	44.4-71.2

Jorge Facao et. al 2011 [89] designed a trapezoidal cavity and by fixing geometry, ray tracing model concluded that 12.5 mm diameter of pipes to accommodate solar energy is sufficient. For optical behavior 50° inclinations walls were optimum. The parameters mainly insulation thickness and receiver depth as 35mm rockwool and 45mm depth considered as optimum. Power law fit for heat transfer coefficient was obtained. Correlated heat transfer coefficient for new cavity was higher than basic CLFR cavities.

R Abbas et. al 2012 [90] studied an innovative linear Fresnel receiver of trapezoidal cavity shape. A range of diameters for absorber tubes are investigated. The different tube diameters are optimized for mass flow rate, radiation intensity as well as inlet temperature. The optimized values reported were 1.4 cm diameter 100 m long tubes with efficiency of 70% for radiation intensity of 8-25 kW/m^2. The design offers cost advantages as well as simple and robust structure.

Sendhil Kumar Natarajan et. al 2012 [91] presented steady state, 2-D, non-Boussinesq, laminar, combined natural convection model. Surface radiation model is also presented. The effect of absorber angle, Grashof number, surface emissivities, aspect ratio and temperature ratio was studied. Correlations for the proposed model was also presented. For aspect ratio and temperature ratio greater than 2.5 and 0.6 resp. heat loss is not significant. Thus the design is concluded for reduced heat loses.

S Flores Larsen et. al 2012 [92] studied heat loss for laboratory prototype of 1.4 m length trapezoidal cavity. Simulations were performed using EnegyPlus software as a replacement for complex CFD. 91% of thermal loss occurred in lower portion of cavity. The coefficient of heat transfers 3.39 to 6.35 W/m^2K for temperature of pipe from 110 to 285 °C was obtained.

Sudhansu S Sahoo et. al 2012 [93] carried out numerical study to investigate trapezoidal cavity with eight absorber tubes. The steady laminar model concluded that radiation heat losses are dominant (80-90%). For fluid flow analysis total Nusselt number correlations were developed. The conclusion was obtained for different cavity depths as well as varying heat transfer coefficient and wall emissivity of absorber tubes.

M Lin et. al 2013 [94] a V-shaped cavity of LFR collector is investigated both experimentally as well as numerically. Thermal performance is depicted by calculating variation of heat transfer coefficient with respect to absorber wall temperature. Experiment concluded coefficient of 6.25-7.52 W/m^2K for temperature range 90-150 °C. 12% deviation for numerical results with that of experimental values. Thermal efficiency reduced from 45 to 37% as temperature increased from 90 to 150 °C.

Sudhansu S Sahoo et. al 2013a [95] investigated study state hydro-thermal analysis of trapezoidal cavity receiver. Single and two-phase analysis was carried out. Various parameters like two-phase coefficient for flow, pressure drop, heat loss etc. was obtained. Higher pressure drop in case of two-phase was reported. With increase in mass flux as DNI decreases, pressure drop increases with constant quality steam. As quality of steam is greater than 0.7, flow boiling coefficient decreased.

K.S. Reddy et. al 2014 [96] investigated medium temperature (400 °C) trapezoidal cavity used in LFR plant. Optimization of cavity was achieved using numerical methods. It was obtained that

insulation thickness 300 mm aspect ratio 2 are optimum cavity dimensions. The emissivity is not significant in total heat losses when compared with other parameters.

Izuchukwu F. Okafor et. al 2014 [97] carried out numerical investigations to determine the effect of heat flux on heat transfer coefficient of linear Fresnel collector. Sinusoidal and uniform heat flux was discussed for compound parabolic as well as trapezoidal type receiver. It was concluded that internal heat transfer coefficient is invariable with different outer heat flux. Overall and average heat transfer coefficient increased with decreased thickness and tube diameter. However, reduced diameter may result in higher pressure drop.

Guangdong Zhu et. al 2014 [3] described state-of-the-art linear Fresnel technology with emphasis on utility-scale power plants. The performance, future aspects as well as technology is detailed. Low profile setting was reported advantageous as compared to parabolic trough technology. It offers increasing concentration ratio, lower wind loads, lowers operation and maintenance etc.

Jie Zhu et. al 2014 [98] proposed semi parabolic Linear Fresnel reflector (SPLFR). It was obtained from ray tracing model that parabolic trough efficiency is achieved with new design. Ground usage is similar to LFR system. Eddies on side of pipes elevates heat transfer from walls to fluid in absorber pipes.

M.A. Moghimi et. al 2015 [99] obtained combined optimization for 2-D trapezoidal cavity receiver. Conjugate analysis was done for the heat losses. Cavity depth and insulation dimensions was reported as the most significant parameter for optimization. Greenhouse effect of glass window is obtained using Discrete Ordinate method.

Ashish Saxena et. al 2016 [100] carried out study for trapezoidal cavity with coupled heat loss (convective and radiative). Non-dimensional correlations were developed. Radiation-conduction as well as the Nusselt number external is proposed in correlations.

Hani Beltagy et. al 2017 [101] investigated secondary reflector type Fresnel receiver. Analytical study and experimental measurements are in accordance. An efficiency value for daily basis of 40% was achieved for 250kW prototype plant.

CHAPTER-IV

4 Scope of the study

Investigation on CLFR technology has got a vast scope. Since this is a new technology which is under optimization stage. There are various parameters that need to be optimized in order to get higher efficiency and performance. The main scope is:

- Solar flux needs to be concentrated with higher efficiency. This will lead to higher overall efficiency according to thermodynamic laws.
- Conjugate study need to be carried out. This will lead to better understanding of heat losses associated with the cavity.
- Conduction, convection as well as radiation loss can be minimized once determined the causes for the same.
- Different heat transfer mechanisms can be achieved to increase heat transfer between wall of absorber and HTF.
- Fluid flow pattern need to obtained both in case of internal absorber flow as well as the pattern of cavity air flow.
- Various socio-economic studies have to be carried out along with different policies related to this technology.

CHAPTER-V

5 Objective of the study

The trapezoidal cavity is investigated to be used in CLFR power plant. A three-dimensional approach with conjugate analysis is tried. This leads to results that are near to our real world issues as well as applications. The main objectives are:

- Optimization of trapezoidal cavity.
- Insulation thickness, depth of cavity, orientation of absorber tubes is investigated.
- Best possible configuration is tried to be found out.
- Different heat losses are calculated.
- Fluid flow through absorber tubes as well as cavity air due to gravitational effects is analyzed.

CHAPTER-VI

6 Research Methodology

The investigation is carried out for a three dimensional trapezoidal cavity. The methodology followed is as follows:

- Recent technology that is renewable, clean as well as quickly curb the greenhouse gases is chosen.
- The potential of development of technology is sought.
- Literature studies have been carried out.
- Problem identification with the current technology is found.
- The cavity is taken and optimization studies in terms of heat losses, fluid flow is obtained using simulation environment FLUENT (ANSYS WorkBench Package).
- Various heat losses are found with conjugate analysis.
- Different fluid behavior is found in two different studies.
- Configuration of absorber pipes is investigated.
- Results and discussions are presented.

CHAPTER-VII

7 Result and Discussions

7.1 Study on the heat loss characteristics of staggered aligned absorber tubes

There have been numerous studies in the literature optimizing CLFR plant focusing on various parameters like temperature, orientation, the geometry of receiver etc. The study carried out without any secondary reflector concluded the use of multi-pipe cavity receiver for LFR plant [62]. In 2004, the trapezoidal cavity was proposed enhancing LFR performance [50]. Henceforth, the research focus shifted towards geometrical aspect of trapezoidal cavity. The study was performed for width (500 to 1200 mm) and depth (100 to 300 mm) of cavity receiver [102]. The cavity width was considered to be 160 mm whereas 50 to 150 mm variation in depth was considered [103]. The heat optimizing parameters for different width (96 mm) and depth varied from 25 to 65 mm [104]. These studies carried out reporting interaction among different variables was not evident i.e. effect of cavity depth and angle of geometry considered on heat losses [93]. Further the geometrical parameters that affect thermal performance are insulation thickness and material [93]–[95]. There have been rare studies on the arrangement of absorber pipes.

The present study mainly focusses the thermal losses that are taking place inside receiver cavity. Therefore, staggered arrangement of absorber tubes is studied in order to investigate the flow pattern and heat losses associated. In order to facilitate the study, computational software package ANSYS WorkBench (WB) was employed [105]. Thermal losses taking place due to the blowing wind under glass aperture of receiver cavity as well as the effect of coating on absorber pipes with different operating ranges for temperature are investigated. Further, different fluid flow patterns are determined due to natural convection inside receiver cavity.

Receiver description*:*

In the present study, staggered receiver cavity is modeled with symmetry conditions as shown in Figure 7.1 (a). Pipe diameters are chosen according to NPS1 standards (SS 304 material). Conduction is not considered in the present study. Numerical investigations are performed on the air present inside the cavity.

Numerical analysis

Model description

The cavity side wall and top wall are considered insulated. The computational domain is further divided into elements by using mesh function of ANSYS WorkBench package. The meshing module generates a total of 8822 elements. The cavity is defined by unstructured grid since the geometry is complex. The quality of mesh generated is validated according to set criteria [106]. The mesh model is shown in Figure 7.1 (b). The continuity, momentum and energy equations are solved for the analysis:

Continuity equation

$$\frac{\partial(\rho u)}{\partial x} + \frac{\partial(\rho v)}{\partial x} = 0 \tag{1}$$

Momentum equation

$$\left(u\frac{\partial u}{\partial x} + v\frac{\partial u}{\partial y}\right) = -\frac{1}{\rho}\frac{\partial P}{\partial x} + \vartheta\left(\frac{\partial^2 u}{\partial x^2} + \frac{\partial^2 u}{\partial y^2}\right) + g\beta(T - T_h) \tag{2}$$

Energy equation

$$\left(u\frac{\partial T}{\partial x} + v\frac{\partial T}{\partial y}\right) = \alpha\left(\frac{\partial^2 T}{\partial x^2} + \frac{\partial^2 T}{\partial y^2}\right) \tag{3}$$

Since the temperature range chosen for the numerical analysis (350K to 550K) obtains a factor greater than 0.1 (for Boussinesq approximation). Therefore, the air in the cavity is assumed to be an ideal gas. Conjugate analysis (convection and radiation) is performed computationally. Surface to surface (S2S) model is chosen for calculating radiation thermal loss. S2S is coupled with natural convection model and is widely used model for non-participating working fluid (absorption, emission and scattering). Grey and diffuse surface is the main assumption besides the view factors which account for orientation, size and distance influence on thermal losses.

Boundary conditions:

Various boundary conditions such as walls are considered with no slip conditions and insulated (top and side wall). From the literature, the absorber tubes are considered subjected to constant isothermal temperature (350K to 550K) condition [102], [106]–[108]. Insulation for side and top wall is considered in order to reduce heat losses i.e. adiabatic conditions are chosen [100]. Since, high-temperature walls emit radiation hence cavity walls (Ɛ=0.1, absorber wall with Ɛ=0.5 to 0.9)

are considered with radiation conditions. Moreover, glass bottom is chosen with convection (h=5 to 25 W/m^2K) and radiation conditions (Ɛ=0.9) since convection is dominant with glass bottom wall.

Numerical procedure:

Fluent 15 software package is employed to generated results of numerical analysis. Laminar natural convection is used for flow model. Pressure-velocity coupling equation is discretized using Second Order Upwind Scheme. 10^{-3} and 10^{-6} are assumed for residuals. The convergence is concluded monitoring heat transfer loss as well as residual levels. Only after reaching steady state conditions the solutions are obtained.

Mesh generation:

A particular geometry of cavity receiver is used in ANSYS Workbench to generate the mesh. The triangular method of meshing is applied as the geometry is complex and concentrated mesh can be produced near circular faces. For automatic mesh generation, Physics preferences were chosen CFD, Solver Preference as Fluent and 100 is set for Relevance. Relevance center along with smoothing is chosen fine with curvature normal angle being 7° and Growth Rate as 1.05 [109]. Further, the grid is generated with maximum skewness of 0.55 (<0.83 as suggested by Bakker), the maximum aspect ratio of 2.37 as well as average orthogonal quality near to unity i.e. 0.96. Figure 7.1 (b) shows the mesh model.

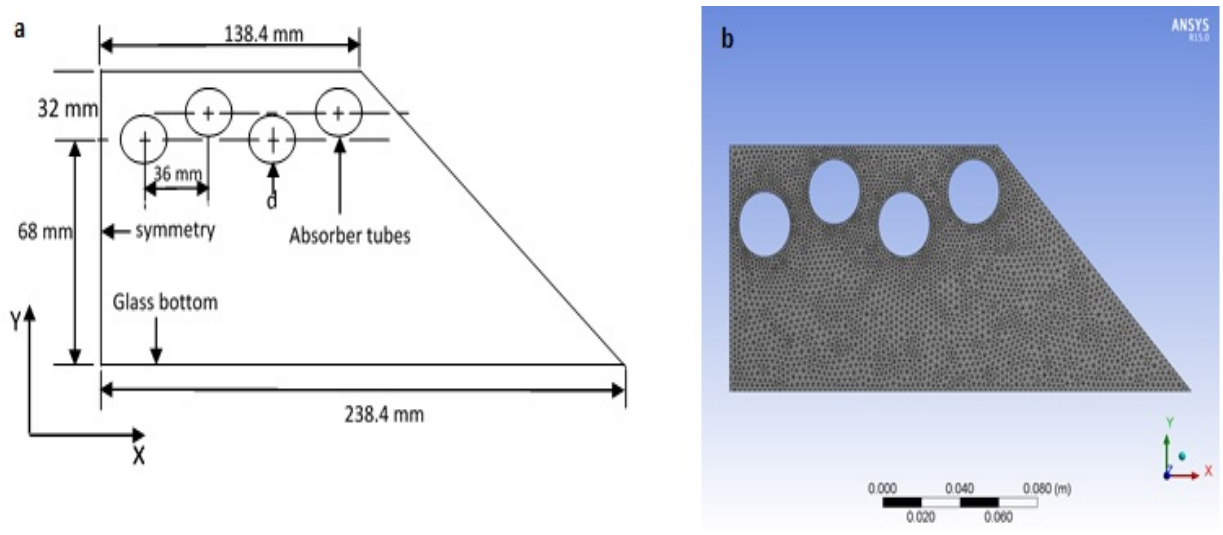

Figure 7.1. (a) Cavity sketch and (b) mesh model.

Results and discusions

Isotherms and flow patterns:

Cavity isotherm contours for h=10 W/m^{2}K as well as streamlines for absorber temperature of 550 K and emissivity 0.8 are shown in Figure 7.2. From isotherm contours it can be observed that horizontal temperature gradient is not present i.e. temperature profile is uniform. However, in the vertical direction, there is a significant temperature gradient. Due to convection current where hot air rises above and cold air settles down near the glass wall. Almost upper half of cavity is at a higher temperature than the zone which is near to glass wall showing the effect of blowing wind producing the cooling effect. Similarly, as the blowing wind near glass wall is at the higher velocity the convection current inside the cavity is also at higher velocity. For a higher convection coefficient vortices are generated and average velocity magnitude is higher for increased values of heat transfer coefficient.

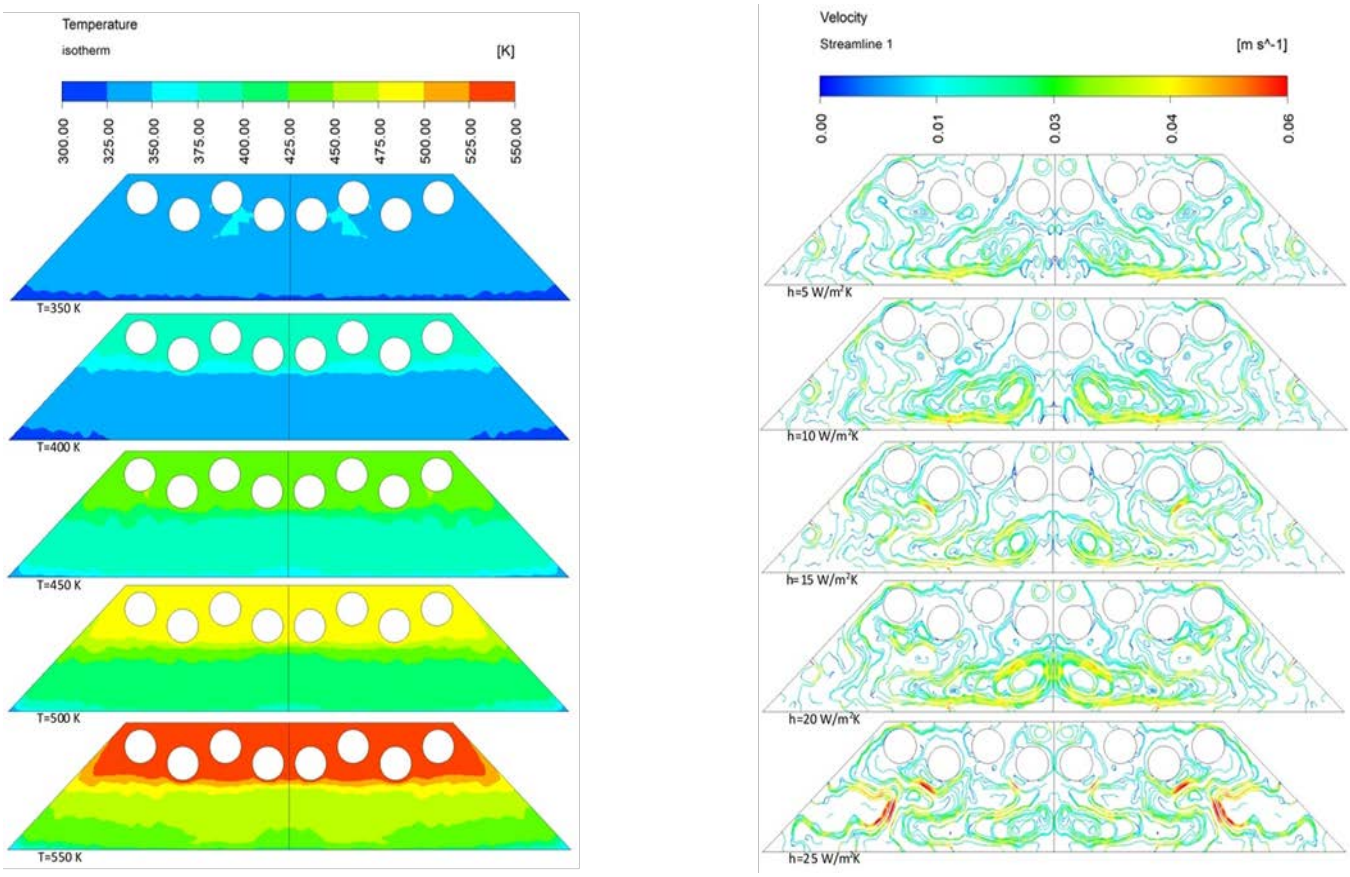

Figure 7.2. Cavity isotherm and streamlines for different temperature and heat transfer coefficient.

Cavity heat exchange:

Figure 7.3 (a) shows heat loss as the temperature is increased from 350 K to 550 K with h=10 W/m^2K and emissivity as 0.8. Heat losses are increased as absorber wall temperature is increased. For a constant absorber temperature (550 K) and h=10 W/m^2K, heat loss variation is presented

with varying coating of absorber tubes in Figure 7.3 (b). Similarly, with the varying wind blowing effect at a constant temperature of 550 K and 0.8 as emissivity, heat losses variation is seen in Figure 7.3 (c). Further, the arrangement effects (staggered) on heat losses with respect to different pipe position is shown in Figure 7.3 (d). It can be seen that heat losses are increased with increased wind blowing effect and coating on absorber walls. Further, the significant dominance of radiation heat transfer can be easily seen. At 350 K, radiation losses comprise of 62.8 % of total heat loss which is increased to 87.4 % at 550 K of absorber wall temperature. Convection loss is almost uniform after 400 K as 108.4 W, 124.04 W and 126.4 W at 450 K, 500 K and 550 K respectively. For coating of 0.5 emissivity, 81.5 % of total losses are radiation losses for constant wall temperature 550 K and h=10 W/m^2K which is increased to 88.8 % for the higher value of emissivity (0.9) as can be seen in Figure 7.3 (b). For constant absorber wall temperature of 550 K and emissivity 0.8, convective losses are increased from 11.7% to 14% as heat transfer coefficient is increased from 5 W/m^2K to 25 W/m^2K as can be found from Figure 7.3 (c). The effect of arrangement can be seen from Figure 7.3 (d). For pipe number 2 starting from symmetry, the heat loss is least among all and pipe 4 (adjacent to side wall) follows. Total heat loss for pipe number 2 is 56.7 % lower than the maximum total heat loss for pipe number 3 at constant absorber wall temperature 550 K, h=10 W/m^2K and emissivity as 0.8.

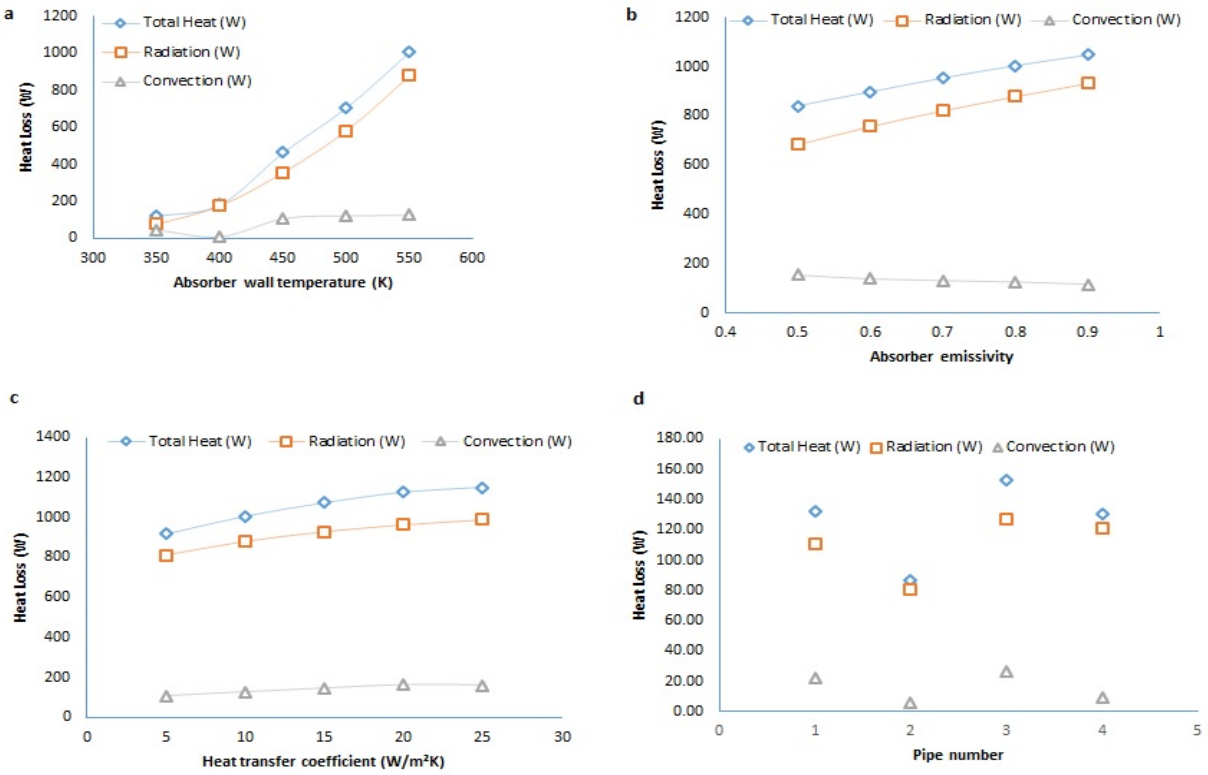

Figure 7.3. Cavity heat exchange with varying (a) absorber wall temperature, (b) absorber wall emissivity, (c) heat transfer coefficient and (d) pipe number.

7.2 Numerical investigation on trapezoidal cavity receiver used in LFR with water flow in absorber tubes

It was observed that in numerical investigations actual HTF flow inside the absorber tubes were not considered. The present study focuses on three dimensional numerical investigations on trapezoidal cavity receiver considering both airside as well as HTF side heat losses. However, only the airside results are included in the present paper.

Receiver description

A symmetric schematic sketch of cavity located at focal point of LFR system is shown in Figure 7.4. The Heat Transfer Fluid (HTF) is taken as water and air is taken inside the cavity. A closed three-dimensional trapezoidal receiver cavity is considered containing eight tubes having a small gap in between allowing thermal expansion. The tubes are of Nominal Pipe Size (NPS) 1 stainless steel (SS) 304 material configuration. There is a glass covering at bottom of receiver cavity to allow solar radiations inside the cavity. The outer covering of other three sides is insulated to

minimize the heat losses. The reflected rays from linear array of mirrors arranged at the bottom falls on the absorber tubes thereby increasing the temperature of HTF flowing.

Numerical analysis

Model description

In the present study, three dimensional model is adopted to predict the heat loss from the receiver cavity. For the purpose of generating mesh as shown in Figure 7.5, the Meshing package of ANSYS 15 Workbench is used. The accuracy and convergence of the solution for the computational domain is checked for skewness and aspect ratio, which should not exceed certain value (0.85) as reported by Bakker [106]. The maximum and minimum values of skewness (max. 0.68 and min. 0.032) and aspect ratio (max. 5.86 and min. 1.10) for present study with the average element quality as 0.811 provides the quality mesh for computational domain.

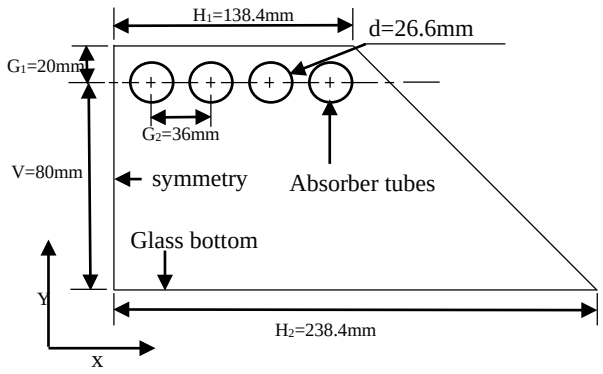

Figure 7.4. Sketch of receiver cavity.

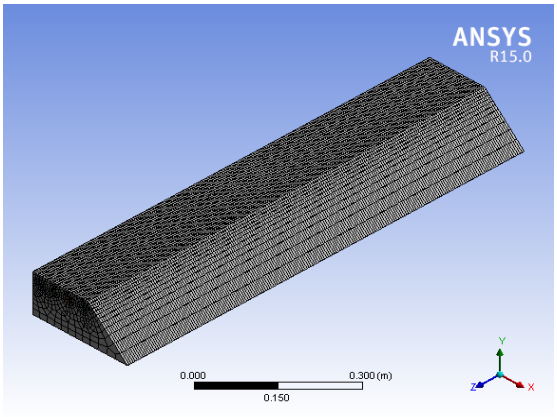

Figure 7.5. Receiver cavity mesh.

The values obtained from numerical simulations are a result of simultaneous solution of the system of flow and heat transfer equations describing mass, momentum, energy. The current work has 350-550 K of temperature range therefore the Boussinesq approximation is invalid. Since, in this temperature range, the product of temperature difference between wall surface and air with the coefficient of thermal expansion of air (0.142-0.58) is higher than 0.1 for Boussinesq approximation to be applied [110]. Hence non-Boussinesq approximation, i.e. the ideal gas characteristics are chosen for cavity air and above equation is used to solve steady, laminar natural convection model. The surface to surface (S2S) radiation model is coupled with natural convection

model. S2S model assumes that the working fluid is not participated in absorption, emission and scattering of radiation. The main assumption of S2S radiation model is that the surfaces are grey and diffuse. However, it should be noted that model assumes heat transfer is affected between two surfaces depending upon their size, orientation and separation distance. View factors are used to account the influence of these variables [105].

Boundary conditions

Different boundary conditions are applied to the cavity receiver. No slip conditions are assumed at walls. Fluids are taken to be incompressible and Newtonian. Since, tubes are continuously subjected to solar radiations therefore tubes are assumed to be at uniform constant temperature after reaching stagnation conditions. Therefore, isothermal boundary conditions are chosen for absorber tubes. The outer covering of cavity receiver is insulated so as to reduce heat losses. Thus, adiabatic conditions are assumed for outer covering. There is radiative heat loss among the walls of receiver cavity due to the high temperature. Moreover, convection losses are significant with bottom glass cover to surrounding air. Hence, both convection and radiation boundary conditions are applied to glass covering. Mainly, top wall, side wall, bottom wall and absorber tube emissivity as 0.1, 0.1, 0.9 and 0.49-0.9 respectively. External emissivity of bottom walls and heat transfer coefficient as 0.9 and 5.0-25.0 W/m^2K. Temperature of absorber tube is varied from 350-550K.

Numerical procedure

The simulation for turbulent incompressible flow are carried out using FLUENT 15 software package. The standard (k-Ɛ) 2-eq model is chosen to model turbulent conditions, since it is most widely used engineering model which includes sub-model for buoyancy [105]. Second order upwind scheme is used for discretization of pressure velocity coupling equations. For residuals of continuity and momentum equations, a convergence criterion of 10^{-3} was imposed whereas 10^{-6} as energy equation residuals. The convergence is determined by the residual levels and also by monitoring relevant integrated quantity like heat transfer coefficient. The solutions are obtained only after satisfying convergence criterion.

Grid independence study

To lower the dependency of grid on the obtained solutions different grids were studied. Since, greater the number of elements, lesser is the deviation in solution. Therefore, different number of

elements are chosen for the grid to check the solution dependency with respect to the grid. The geometry is divided into quadrilateral and hexahedral unstructured mesh elements ranging from 71,050 to 3,35,274. Table 7.1 below shows the variation of total heat transfer with respect to the grid size. It is further seen that the variation in heat transfer solution for elements 71,050 and 1,11,600 is negligible (<1%). Hence, 71,050 elements are sufficient to model the geometry to obtain reliable results. Thereby, reducing the computational time and cost on a greater extent.

Validation and verification of numerical procedure

In order to validate computational results, the simulation values obtained for total heat loss are compared with experimental data obtained by Sahoo et. al. [93] using their cavity lab test setup. It can be seen from Figure 7.6, that the results obtained from simulated data are well in conformation with experimental data.

Table 7.1. Cavity grid study.

Number of elements	Total heat loss (W)	% change in heat loss
71050	106.822	
111600	106.828	0.06
268128	107.830	0.93
335274	107.409	-0.39

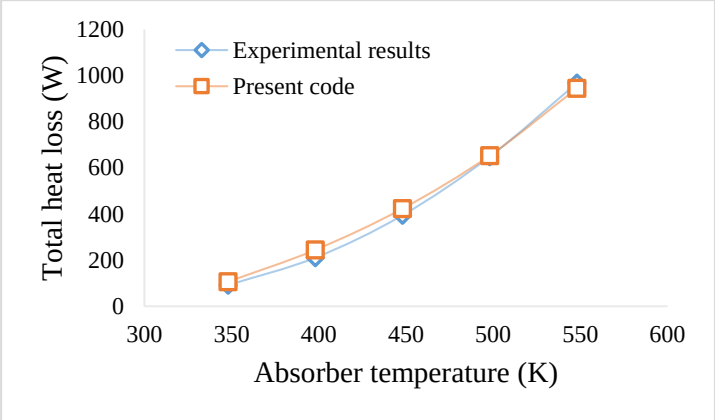

Figure 7.6. Validation study for the simulation problem.

Results

Isotherm contours

Isotherms contours are plotted in Figure 7.7 and Figure 7.8 for various cavity parameters. It can be seen from isotherm contours in Figure 7.7 that temperature variations along horizontal direction is almost negligible and hence uniform profile is seen. However, natural convection is taking place due to the temperature gradient along vertical direction. Thus, rising the air from centre of cavity and settling down from the side surfaces. Further, as the absorber tube temperature is increased the heat affected zone with higher average temperature shifts towards bottom glass cover thereby increasing the vertical temperature gradient. Figure 7.7 (a) shows the approximate average temperature 375.5 K which increases as absorber temperature increases up to 487.5 K. However, the percentage vertical temperature gradient is reduced from 9.09% to 7.14% as temperature varies from 350 K to 550 K respectively this is due to the increased losses at higher temperatures.

It can be observed from Figure 7.8 that as the heat transfer coefficient near glass surface is increased there are significant convective losses. The amount of cooling of air that is taking place near the glass surface as a result of ambient air conditions can be observed easily by varying the heat transfer coefficient. It can be seen that for h=5 W/m^{2}K almost all the entrapped air (90% approx.) is at higher average temperature (480 K approx.). However, the amount of entrapped air with higher temperature is reduced from 90% to approximately 40% with increased value of heat

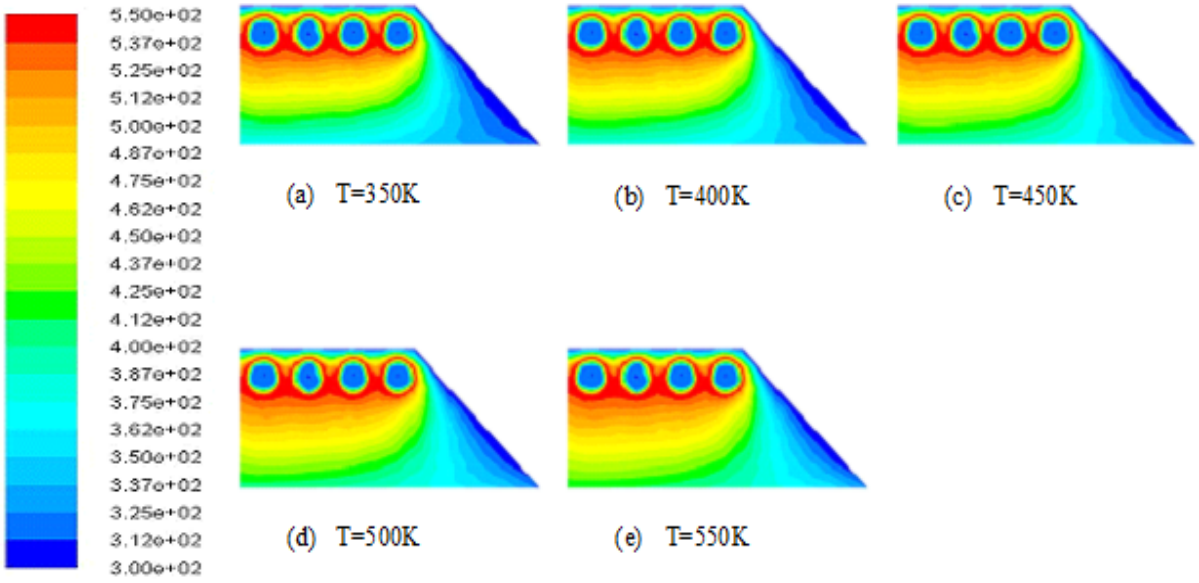

Figure 7.7. Cavity isotherm contours for m=0.1kg/s, h=5W/m2K, Ɛ=0.49 at different absorber temperatures.

transfer coefficient (h=5 to 25 W/m^{2}K). The average temperature is also reduced from 480 K to 360 K as the value of heat transfer coefficient is increased (h=5 to 25W/m^{2}K). It can be concluded from above results that with lesser value of average temperature more heat is being swept away due to blowing wind. Thus, ambient environment conditions significantly affect the heat loss characteristics of the cavity.

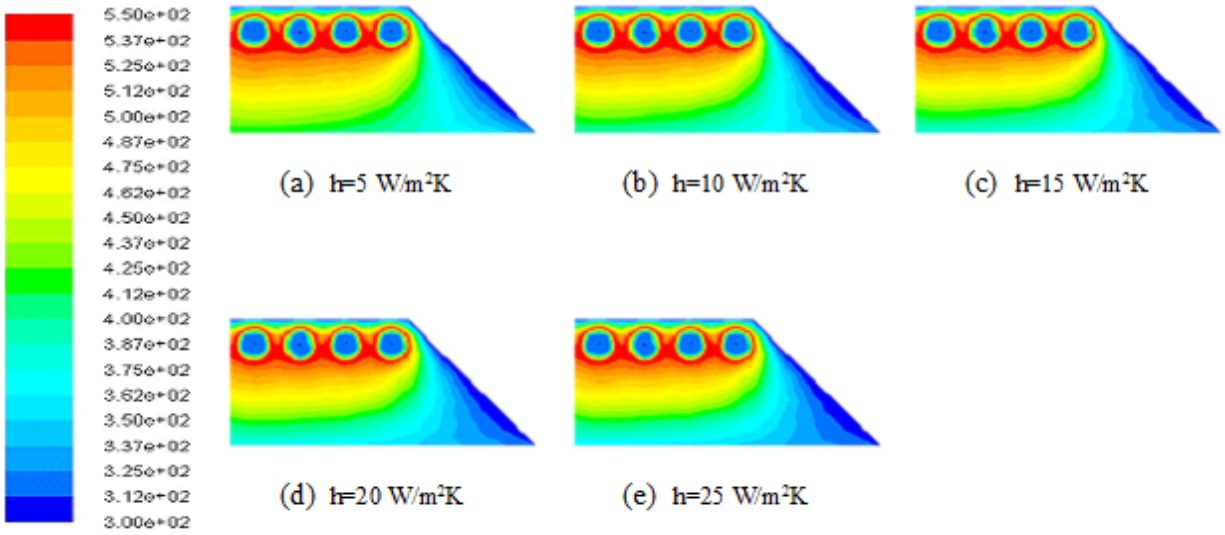

Figure 7.8. Cavity isotherm contours for m=0.1kg/s, Ɛ=0.49, T=550K at different heat transfer coefficient.

Cavity heat exchange

Effect of absorber temperature on heat loss characteristics. Figure 7.9 shows the variation of heat transfer taking place inside the cavity as a function of absorber surface temperature. It is observed that as the wall temperature of absorber tubes increase heat loss is increased for m=0.1kg/s, h=5W/m^{2}K and Ɛ=0.49. Radiative heat loss for temperature 400 K is 244.57 W and for temperature 450 K is 423.32 W showing 87.21% increase in value. The percentage change is decreased from 87.21% to 52.33% as the absorber temperature is increased to 550 K. The convective heat loss amounts to 90.57 W for 400 K and 135 W for 450 K absorber temperature. Thus, there is an increase of 49% in convective losses. This percentage increase changes from 49% to 24.3% as temperature reaches to 550 K. Thus, it is clear that radiative heat losses steep more as compared to convective losses. This is due to the higher temperature of absorber tubes emitting radiation and contributing to radiation losses. It is further observed that at higher absorber temperature (550 K) radiative heat losses are dominant, i.e. 76.45% of the total heat loss for the receiver cavity.

Effect of Rayleigh number - The variation of Nusselt number with respect to Rayleigh number can be observed in Figure 7.10. It is clearly obtained from the graph that Nusselt number is an increasing function of Rayleigh number. As Rayleigh number is increased so does the Nusselt number.

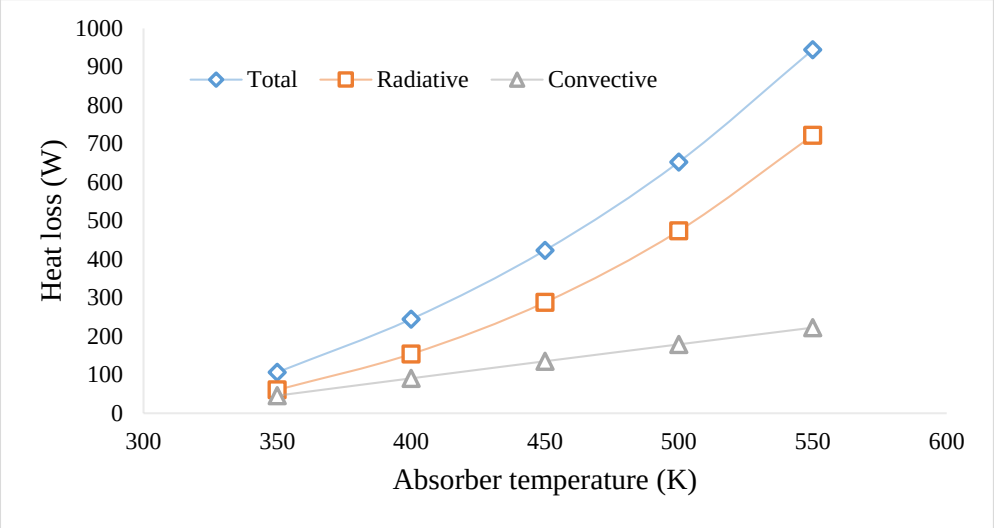

Figure 7.9. Heat loss characteristics (total, radiative and convective) for m=0.1kg/s, h=5W/m2K and Ɛ=0.49.

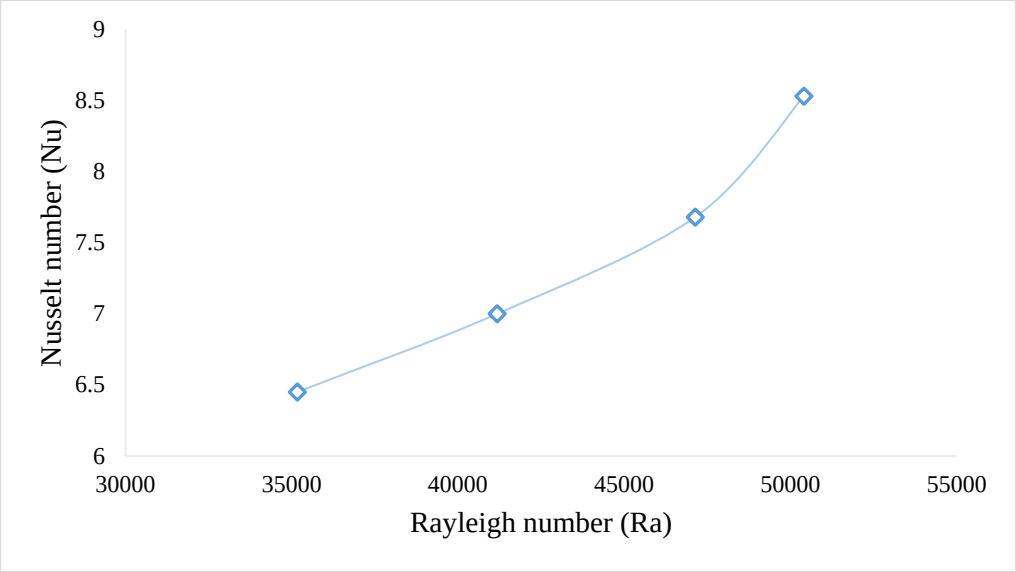

Figure 7.10. Variation of Nusselt number (Nu) for m=0.1kg/s, h=5W/m2K, Ɛ=0.49.

Effect of absorber emissivity. The heat loss characteristics as a function of absorber tube emissivity can be obtained from Figure 7.11. It is observed that convective heat losses are more or less uniform as well as negligible. The radiation losses are dominant as the emissivity values are varied. Radiative heat exchange is increased with increasing values of absorber tube emissivity.

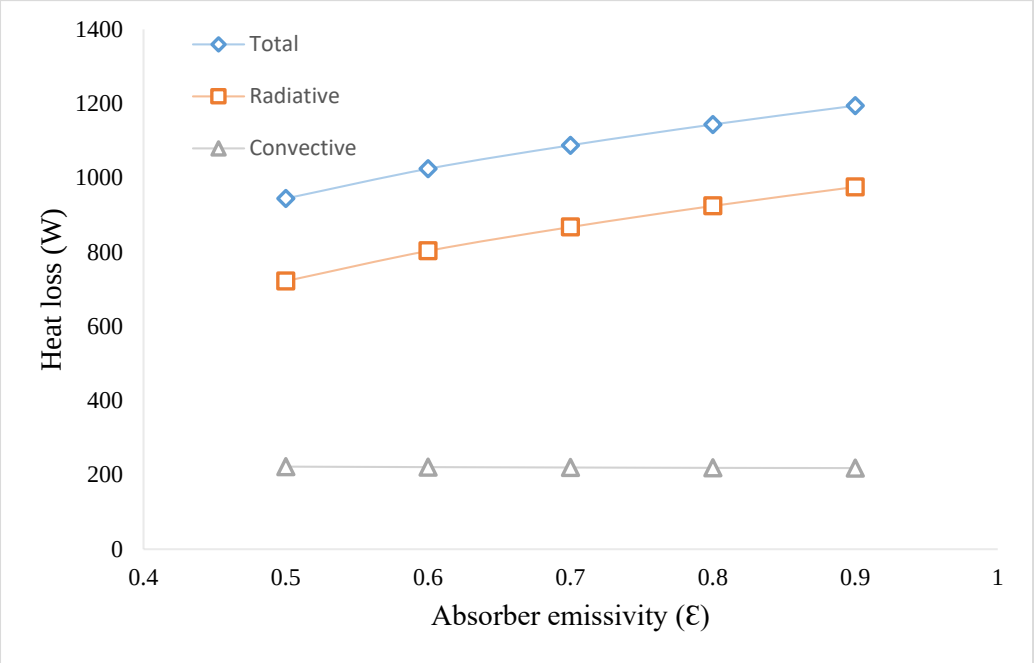

Figure 7.11. Heat loss characteristics (total, radiative and convective) for m=0.1kg/s, h=5W/m2K, T=550.

7.3 Study on thermal performance of different heat transfer fluids used in absorber tubes of a CLFR plant

The efficiency of any plant depends on the components it is made of. Since, Compact Linear Fresnel Reflector (CLFR) plant (advantageous as the stationary absorber, lower mirror heights, separate reflector and receiver system) consist of concentrating system, thermodynamic cycle (coupled with generator), receiver and Heat Transfer Fluid (HTF)/Thermal Energy Storage (TES) as its main components. There had been evidence in literature exploring the effect of HTF as optimizing parameter. Various prototypes [111] had been presented in for gas and fluid HTFs with a challenge of heat transfer between walls and the fluid. Supercritical CO_2 as HTF is increasing interest with Brayton cycle in CSP [112]. Particle suspension system receivers were used in central tower system with various concepts [113], dense particle suspension receiver consists of fluidized particles in suspension and behaves like HTF [114], [115]. For all types of receivers, the heat transfer is an indirect method i.e. HTF receives heat only after absorber walls gets heated. Hence, a temperature limit is introduced and thermal energy exchange limitation gets imposed on HTF flowing. Thus, the heat carrying capacity (inherent property) of HTF impacts thermal efficiency. For these reasons, HTF is a primary component that justifies development and strong research efforts so that performance can be increased.

The key features for selection of HTF [116], [117] are higher thermal stability with the higher working temperature range, low melting point (to avoid solidification in tubes), high thermal conductivity as well as heat capacity, lower viscosity, less corrosion. Therminol VP-1 or Dowtherm A (temperature range as high as 400 °C) were initially used as synthetic oils for CSP plants avoiding phase change and high-pressure requirements for water application as HTF. These fluids when heated above 400 °C produces hydrogen due to molecular breakdown leading to increased makeup fluid requirements. It reduces fluid lifetime produces sludge or byproducts resulting in the reduction of thermal exchange efficiency and increased maintenance. The commercial oils Marlotherm X (Sasol data), Santotherm 59 (Monsanto data), Syltherm XLT (Dow Corning Corporation) and Therminol D12 (Solutia Inc.) were chosen for this study. In order to facilitate the study, computational software package ANSYS WorkBench (WB) was employed [105]. Heat transfer is calculated by varying different parameters like the mass flow rate and inlet temperature. Further, different fluid flow patterns are determined.

Receiver details:

In the present study, 1m long receiver cavity is modeled containing eight tubes with symmetry wall as shown in Figure 7.12 (a). The absorber pipes are SS 304 material with NPS1 as diameter. For thermal expansion, space has been provided between absorber tubes. The HTF is flowing in absorber tubes. Numerical investigations are performed and results are presented for fluid flow behavior.

Numerical study

Model specifications:

The present model is symmetrical and three dimensional with the insulated side as well as the top wall. Mesh function of ANSYS WorkBench package is employed to further divide computational domain into different elements. A total of 1,14,240 elements are generated to obtain the result. The generated grid is validated according to criteria present [118]. The mesh model is shown in Figure 7.12 (b). The continuity, momentum and energy equations are solved for the analysis:

Continuity equation

$$\frac{\partial(\rho u)}{\partial x} + \frac{\partial(\rho v)}{\partial x} + \frac{\partial(\rho w)}{\partial z} = 0 \qquad (1)$$

Momentum equation

$$\left(u\frac{\partial u}{\partial x}+v\frac{\partial u}{\partial y}+w\frac{\partial u}{\partial z}\right)=-\frac{1}{\rho}\frac{\partial P}{\partial x}+\vartheta\left(\frac{\partial^2 u}{\partial x^2}+\frac{\partial^2 u}{\partial y^2}+\frac{\partial^2 u}{\partial z^2}\right)+g\beta(T-T_h) \quad (2)$$

Energy equation

$$\left(u\frac{\partial T}{\partial x}+v\frac{\partial T}{\partial y}+w\frac{\partial T}{\partial z}\right)=\alpha\left(\frac{\partial^2 T}{\partial x^2}+\frac{\partial^2 T}{\partial y^2}+\frac{\partial^2 T}{\partial z^2}\right) \quad (3)$$

The air present in the cavity is chosen with ideal gas assumption. Since the product of temperature difference and average temperature gives the result that is greater than that for Boussinesq approximation to be applicable. Since cavity is subjected to both radiation as well as convection heat transfer. Therefore, Surface to surface (S2S) model is selected for calculating radiation heat loss. S2S includes buoyancy as well as natural convection model is coupled. It assumes fluid to be non-participating medium besides Grey and diffuse surface. View factors are calculated for orientation, size and distance influence on thermal losses.

Boundary conditions and numerical procedure*:*

The cavity is subjected to different boundary conditions. Walls are assumed with no slip conditions as well as insulated. The absorber tube walls are subjected to isothermal temperature (573 K) as assumed in the previous literature [102], [103], [107], [108]. Since radiation losses are dominant for high-temperature walls hence cavity walls (Ɛ=0.1, absorber wall with Ɛ=0.8) are considered [100]. Moreover, glass bottom is assumed to confine the heat from outside wind effects (h=5 W/m^2K) and emissivity (Ɛ=0.9), since convection is dominant with glass bottom wall. The Fluent software package is employed to obtain results of numerical analysis. Pressure-velocity coupling equation is discretized using Second Order Upwind Scheme with momentum and energy is monitored with 10^{-3} and 10^{-6} for residuals. The convergence is concluded monitoring heat transfer as well as residual levels. Solutions are obtained once convergence criteria are met.

Grid independence test:

The cavity grid is shown in Figure 7.12 (c). The independence of grid with respect to the solution obtained is calculated. The percent deviation of solution from initial value is determined. Therefore, Nusselt Number is studied for various mesh sizes having element numbers in the range

of 70,644 to 2,36,680. A total of 1,14,240 elements were sufficient to model the cavity and obtain satisfactory results.

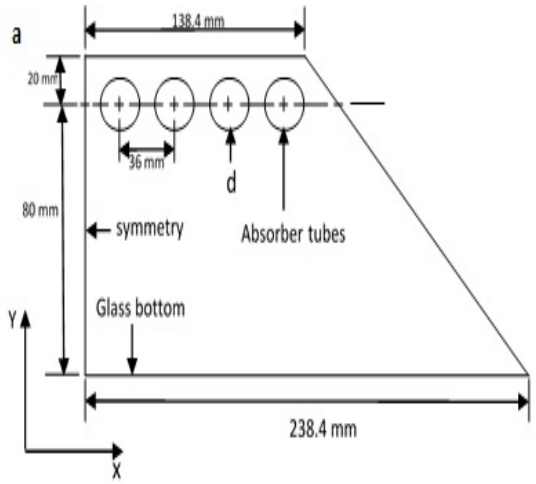

b

Elements	Nusselt Number (Nu)	% deviation
70644	565.29	
114240	525.45	7.05
236680	520.02	1.03

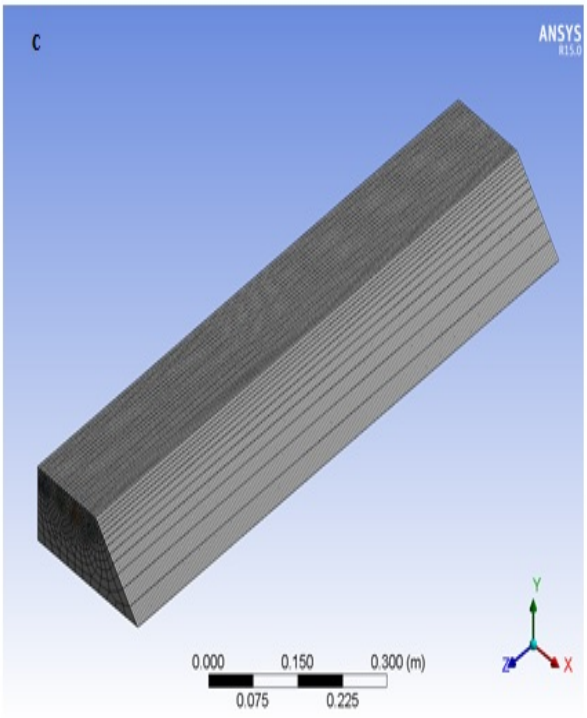

Figure 7.12. (a) Cavity sketch, (b) grid independence test and (c) mesh model.

Results and discussions

Isotherms and flow patterns:

Sample isotherm contours and velocity profile (inlet temperature 80°C) can be seen in Figure 7.13. It can be clearly seen that higher temperature at the outlet is for Marlotherm X. The region that is at higher temperature is similar for Syltherm XLT and Therminol D12. The changes in velocity contours are easily visible. Therminol D12 is at flowing at a higher flow rate followed by Marlotherm X, Syltherm XLT and Santotherm 59.

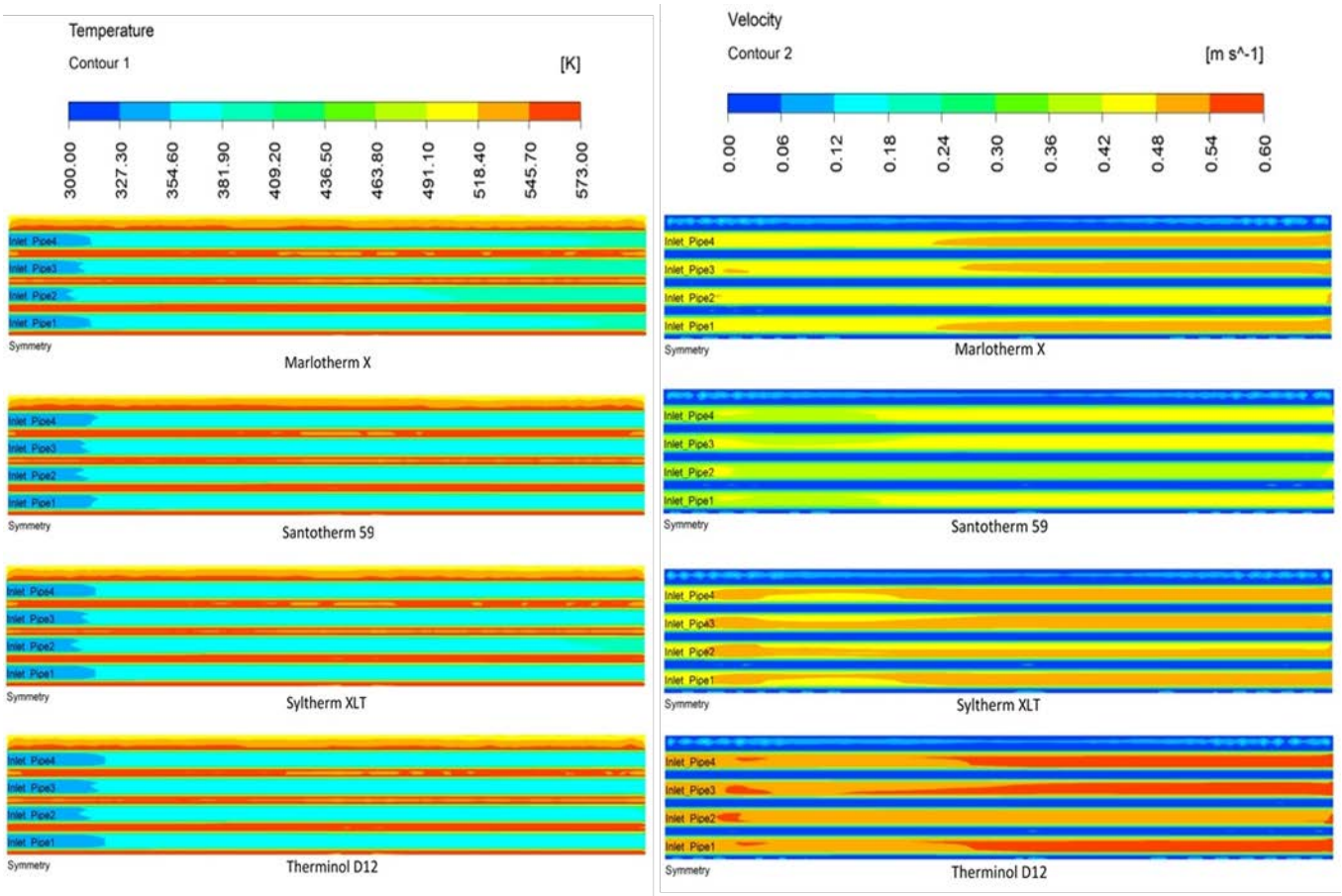

Figure 7.13. Sample cavity isotherm and velocity contours.

Cavity heat exchange:

Figure 7.14 shows temperature rise as a function of inlet temperature and heat transfer associated with varying inlet temperature from 80°C to 200°C. It can be seen that for lower inlet temperature i.e. 80°C the temperature rise is higher as compared to 200°C of inlet temperature for each fluid keeping mass flow rate 0.2 kg/s and absorber wall temperature 573 K as constant. The outlet temperature obtained at 80°C of inlet temperature are 119.72°C, 109.65°C, 106.77°C and 96.48°C for Marlotherm X, Syltherm XLT, Therminol D12 and Santotherm 59 respectively. However, at 200°C inlet temperature, outlet temperature for Marlotherm X, Syltherm XLT, Therminol D12 and Santotherm 59 is 218.22°C, 215.43°C, 214.81°C and 215.19°C respectively. The temperature rise is reduced from 39.72°C, 29.65°C, 26.77°C and 16.48°C for Marlotherm X, Syltherm XLT, Therminol D12 and Santotherm 59 to 18.22°C, 15.43°C, 14.81°C and 15.19°C respectively keeping absorber wall temperature (573 K) and mass flow rate (0.2 kg/s) as constant by varying

inlet temperature from 80°C to 200°C. The temperature rise is maximum for Marlotherm X at all values of inlet temperature followed by Syltherm XLT, Therminol D12 and Santotherm 59. There is 49.87% reduction in temperature rise for Marlotherm X as inlet temperature in increased from 80°C to 200°C. However, heat transfer is highest for Therminol D12 followed by Marlotherm X, Santotherm 59 and Syltherm XLT. There is 35.53% increase in heat transfer from Therminol D12 as the inlet temperature is increased from 80°C to 200°C. Further, for the inlet temperature of 200°C least heat transfer is shown by Syltherm XLT which is 24.5% lesser than Therminol D12 at the same temperature.

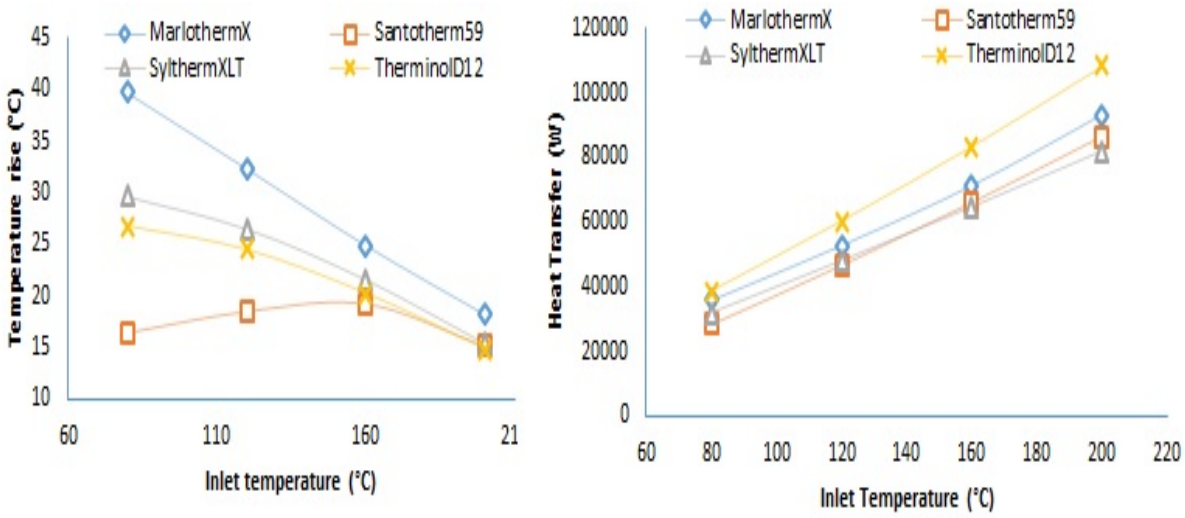

Figure 7.14. Cavity heat exchange with varying inlet temperature.

7.4 Numerical analysis of synthetic fluids in three-dimensional trapezoidal cavity used for CLFR plant

HTF is one of the major component as large quantity HTF is required to drive CSP plant, hence performance needs to be maximized. The high temperature HTF can be stored and utilized to produce power when there is no sunlight. The main characteristics of HTF may be summed up as [119], [120]:

- Low melting point
- High boiling point
- High thermal stability
- Low vapour pressure at high temperature (<1 atm)

- Low viscosity
- High thermal conductivity
- Higher heat storing capacity
- Low corrosion rate with metals

Heat transfer fluids (HTF) are being used in Concentrating Solar Power (CSP) applications viz. Mineral oil, silicone oil and synthetic oil. A recent reviews shares commercial solar thermal power station around the world with thermal oils as HTF [121]. The properties are almost similar mainly 0.1 W/mK thermal conductivity for three of above classifications [122]. Xceltherm 600, a paraffinic, non-toxic mineral oil developed by Radco Industries Inc. is used in Saguaro CSP plant at Redrock, in Arizona, USA [123]. The stability of these thermal oils are up to 673 K and hence used in high temperature as well as highly efficient thermal plants [121], [124]. Medium temperature solar application incorporated Dow-corning 550 with better heat transfer behavior as compared to water [125]. Since, advantage of using HTFs are the constant thermal conductivity over a wide range of temperature however, low specific heat capacity leads to higher pumping power [125]. The performance of parabolic trough collector (PTC) with 7 different thermal oils is studied [126]. It was found that oils (Syltherm XLT, Syltherm 800, Marlotherm X, Marlotherm SH, Santotherm LT, Santotherm 59 and Therminol D12) have optimum working temperature range of around 573 to 673 K. Various new promising applications of using Linear Fresnel Reflector (LFR) plant in increasing working temperature range is explored (540°C) [127]. The economy affecting study of different HTFs had been done for parabolic trough concentrating solar technology [128]. To best of our knowledge there are rare studies with different HTF behavior in absorber tubes with three-dimensional trapezoidal receiver cavity used in Compact Linear Fresnel Reflector (CLFR) plant.

Hence, the present numerical study is carried out to predict the flow behavior as well as heat transfer characteristics of the heat carrying fluid flowing in absorber tubes.

Receiver Description

In present study a three dimensional symmetric model is chosen to reduce computational time and cost. The sketch of the cavity is shown in Figure 7.15, with dimensions in mm.

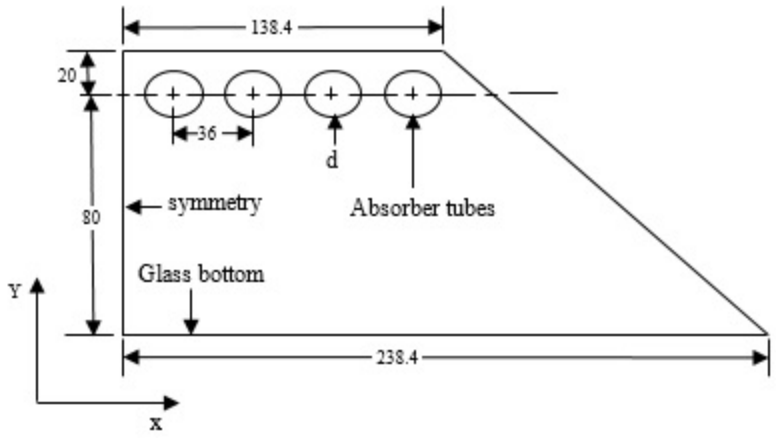

Figure 7.15. Trapezoidal receiver cavity sketch.

Cavity consists of eight tubes of SS 304 configuration and diameter as NPS1. There is a gap provided between tubes to allow for thermal expansion of material. Heat transfer Fluids flow through absorber tubes taking heat from the glass aperture. The cavity glass bottom wall entraps air and serves in reducing the effect of outer atmospheric conditions.

Numerical analysis

Model and mesh description

Numerical analysis for the thermal losses is done for three-dimensional cavity with different heat transfer fluid flowing through absorber tubes. Mesh is generated with 1,14,240 elements using ANSYS WorkBench module [105] as shown in Figure 7.16. The criteria used to validate the mesh is obtained from literature [106]. Skewness as well as aspect ratio and average element quality is well under limits. The solution to the numerical analysis is obtained using simultaneously solving energy momentum equation [93] below:

Continuity equation

$$\frac{\partial(\rho u)}{\partial x}+\frac{\partial(\rho v)}{\partial y}+\frac{\partial(\rho w)}{\partial z}=0 \qquad (1)$$

Momentum equation

$$\left(u\frac{\partial u}{\partial x}+v\frac{\partial u}{\partial y}+w\frac{\partial u}{\partial z}\right)=-\frac{1}{\rho}\frac{\partial p}{\partial x}+\vartheta\left(\frac{\partial^2 u}{\partial x^2}+\frac{\partial^2 u}{\partial y^2}+\frac{\partial^2 u}{\partial z^2}\right)+g\beta(T-T_h) \qquad (2)$$

Energy equation

$$\left(u\frac{\partial T}{\partial x}+v\frac{\partial T}{\partial y}+w\frac{\partial T}{\partial z}\right)=\alpha\left(\frac{\partial^2 T}{\partial x^2}+\frac{\partial^2 T}{\partial y^2}+\frac{\partial^2 T}{\partial z^2}\right) \quad (3)$$

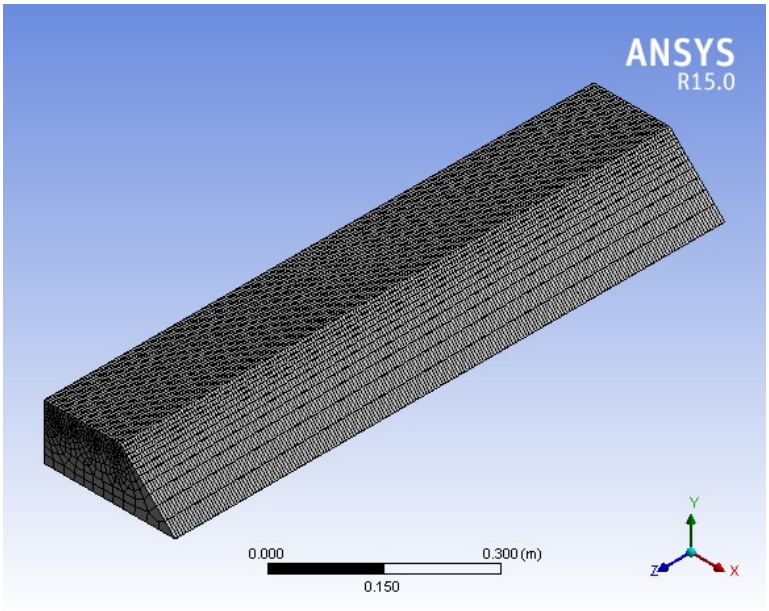

Figure 7.16. Trapezoidal cavity model mesh.

Since ideal gas assumptions are applied for solution of steady laminar natural convection model. As Boussinesq approximation is not valid for the above temperature range (573 to 723 K). The product of wall temperature difference and thermal expansion coefficient gives a value higher than 0.1 as per Boussinesq approximation [110]. To calculate radiation heat transfer surface to surface (S2S) model is invoked. S2S considers natural convection and assumes non participating medium (in absorption, emission and scattering of radiation). Surfaces are assumed to be gray and diffuse as well as heat loss mainly affected by parameters like orientation, size and distance of surfaces. Such parameters are accounted in view factors [105].

Boundary conditions and numerical procedure

The cavity is subjected to various boundary conditions. Walls of the cavity are applied with no slip conditions. Incompressible and Newtonian fluids are taken. Constant temperature conditions (573 to 723 K) are applied to absorber walls since after reaching steady conditions solar flux makes temperature uniform throughout absorber tube walls. Cavity side wall and top wall is assumed insulated since for complex geometry this kind of assumption increases simplicity, adiabatic conditions are applied. Conjugate study (convection and radiation) is performed as high

temperature surfaces are subjected to radiation losses and fluid solid interaction results in convection losses. Top wall as well as side wall have an emissivity value of 0.1 whereas glass bottom has 0.9 as internal and external emissivity. Absorber tubes are assumed coated, emissivity 0.8 as well as inner emissivity 0.45. Heat transfer coefficient at glass wall is taken to be 5 W/m^2K. FLUENT software package is used for simulating laminar and turbulent flow in absorber pipes. Widely adopted turbulent k-Ɛ 2-eq model is chosen as it accounts for sub-model of buoyancy [105]. The equation residuals for energy and momentum are 10^{-6} and 10^{-3} respectively as well as solution was obtained depending upon residual values and monitoring static average temperature at the outlet of absorber tubes. Table 7.2, shows the properties of different HTF used in present numerical study.

Table 7.2. Heat Transfer Fluid properties.

Heat Transfer Fluid	Thermal conductivity (W/mK)	Specific Heat Capacity (kJ/kgK)	Dynamic Viscosity (Pa.s)	Density (kg/m3)
Addinol XW15	0.133	1.322	0.02653	880.3
Shell Heat Transfer Oil S2	0.133	1.915	0.056	855
Dowtherm A	0.1371	1.601	0.00325	1051.7

Grid independence study

Since grid i.e. number of elements largely affects the solution obtained hence a study is incorporated in order to eliminated the dependency of grid on the obtained solutions. Therefore, different grid with unstructured hexahedral and quadrilateral elements is generated using automatic mesh generation [109] tool of Meshing package in ANSYS WorkBench. The different number of elements ranging from 70,644 to 2,68,416 are chosen as shown in Table 7.3, and average temperature

of outlet for heat transfer fluid is studied for variation. Since, deviation is less than 1% therefore, grid consisting of 1,14,240 elements is chosen to obtain results. Thus, computation study is carried out with accuracy and in less time.

Table 7.3. Grid independence study.

No. of elements	Absorber outlet temperature (K)	% Deviation
70644	302.55	
114240	304.92	0.78
268416	307.00	0.68

Results

Isotherm contours

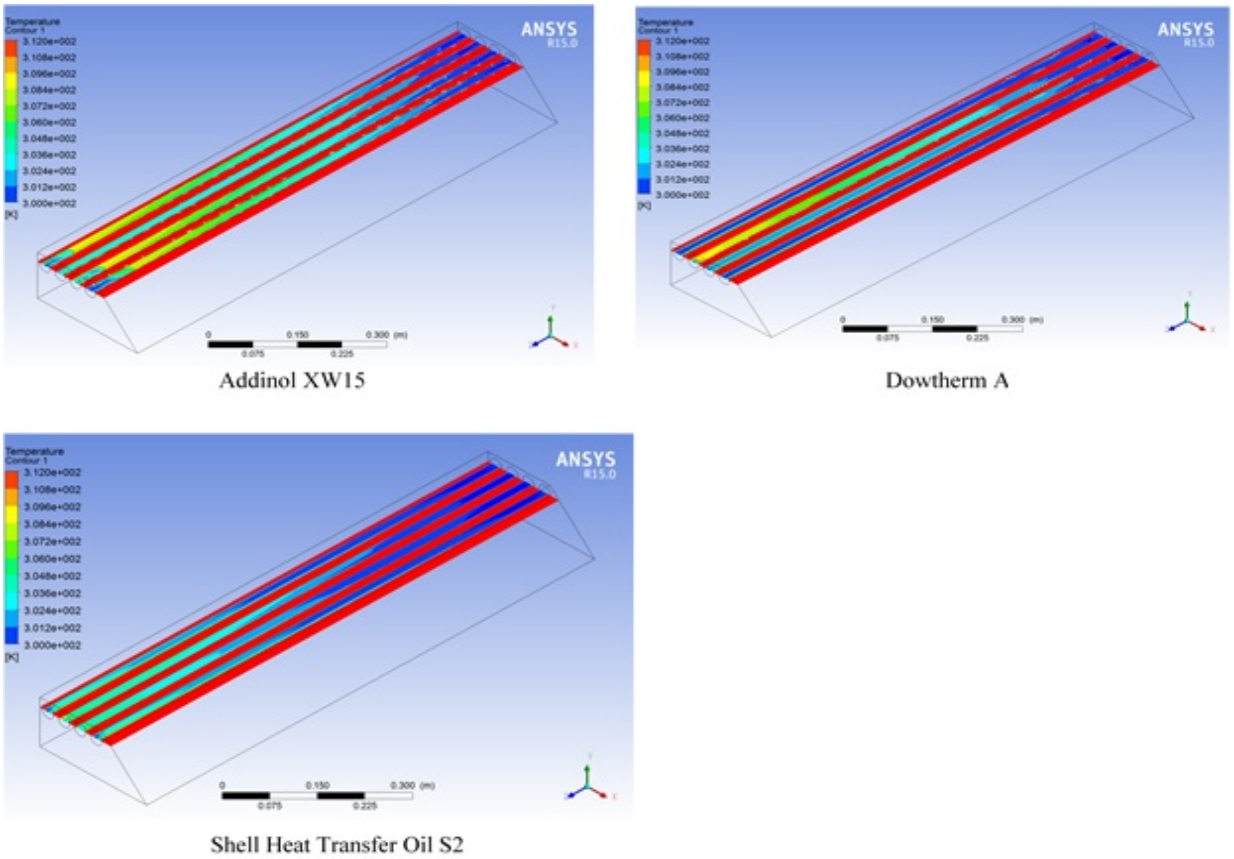

Figure 7.17. Sample isotherm contours for three heat transfer fluids viz. Addinol XW15, Shell Heat Transfer Oil S2 and Dowtherm A.

Higher outlet fluid temperature is observed for addinol XW15 operated at absorber wall temperature 573 K and mass flow rate 0.1 kg/s Figure 7.17. the axial variation of HTF inside the absorber tubes are observed to be different based on its position inside the CLFR cavity. This is due to the different heat interactions of cavity walls.

Cavity Heat Exchange

Heat transfer is calculated for different absorber wall temperature 573 K to 723 K in steps of 50 K. Figure 7.18, Figure 7.19, Figure 7.20, Figure 7.21, Figure 7.22, shows the thermal performance of different heat transfer oils. At low flow rate of 0.1 kg/s, the heat carrying capacity is found to be varied within 8.25% as shown in Figure 7.18. For a flow rate of 0.2 kg/s, major increase in thermal performance of HTF is observed for Dowtherm A. This is due to lower viscosity of Dowtherm A, which makes the flow turbulent for 0.2 kg/s of mass flow rate. Similar trend can be seen for higher mass flow rate 0.25 kg/s. Figure 7.19, shows heat transfer variation for mass flow rate 0.1 kg/s for different HTF. As the temperature increases for absorber wall from 573 K to 723 K the heat transfer is increased by 44.9% approximately for Shell Heat Transfer Oil S2, 49.7% for Addinol XW15 and 48.04% for Dowtherm A. However, the heat exchange for Addinol XW15 is lower as compared to other HTF. Similar, trend is exhibited for a mass flow rate value of 0.15 kg/s, Addinol XW15 being the lowest among all three HTFas shown in Figure 7.20. For a mass flow rate of 0.2 kg/s in Figure 7.21, and 0.25 kg/s in Figure 7.22, turbulent

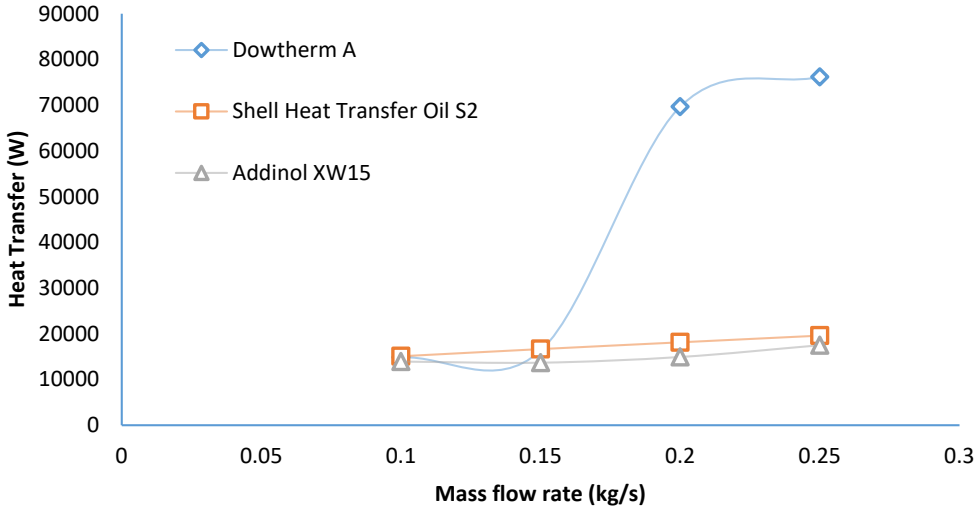

Figure 7.18. Effect of mass flow rate on heat transfer for absorber wall temperature T=573 K.

characteristics are observed for Dowtherm A therefore the heat that is exchanged is significantly higher as compared to higher viscosity HTF. The anomalous heat transfer characteristics due to turbulence are explained in literature [129]–[132]. The increase for Dowtherm is steeper than Shell Heat Transfer Oil S2 HTF, 51.6% for mass flow rate 0.2 kg/s and 50% increase for flow rate of 0.25 kg/s which is 46.3% and 45.02% for Shell Heat Transfer Oil S2 respectively. The increase shown for Addinol XW15 is 55.47% and 38.2% approximately for mass flow rate of 0.2 kg/s and 0.25 kg/s respectively.

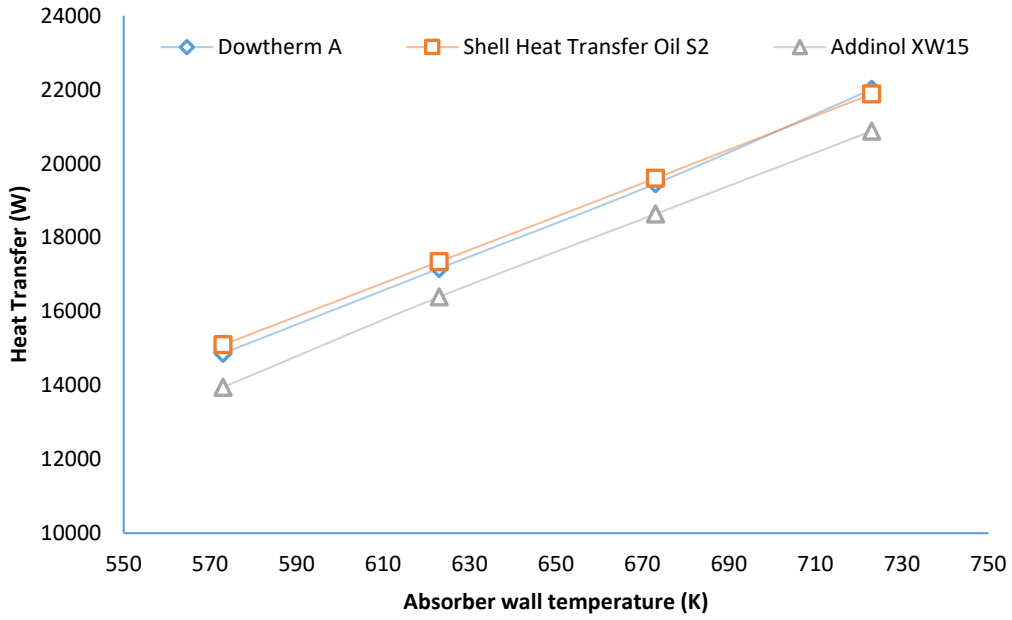

Figure 7.19. Effect of absorber wall temperature on heat transfer for mass flow rate 0.1 kg/s.

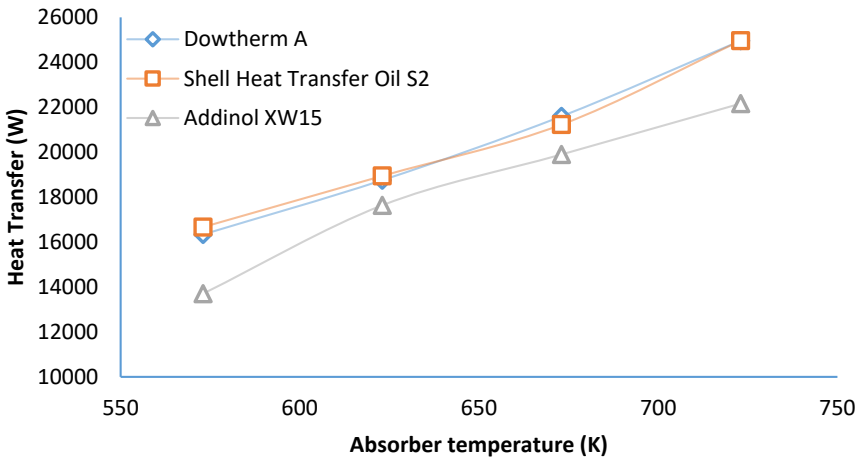

Figure 7.20. Effect of absorber wall temperature on heat transfer for mass flow rate 0.15 kg/s.

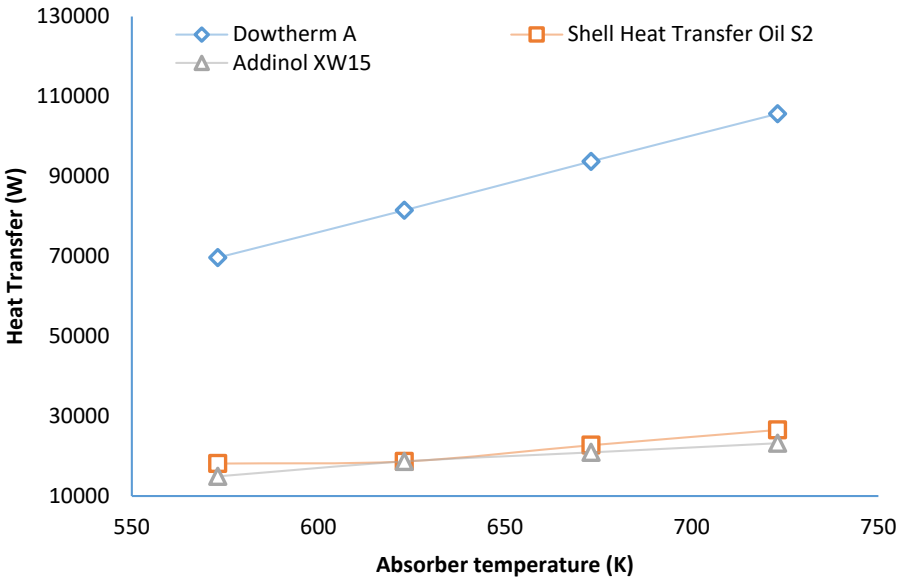

Figure 7.21. Effect of absorber wall temperature on heat transfer for mass flow rate 0.2 kg/s.

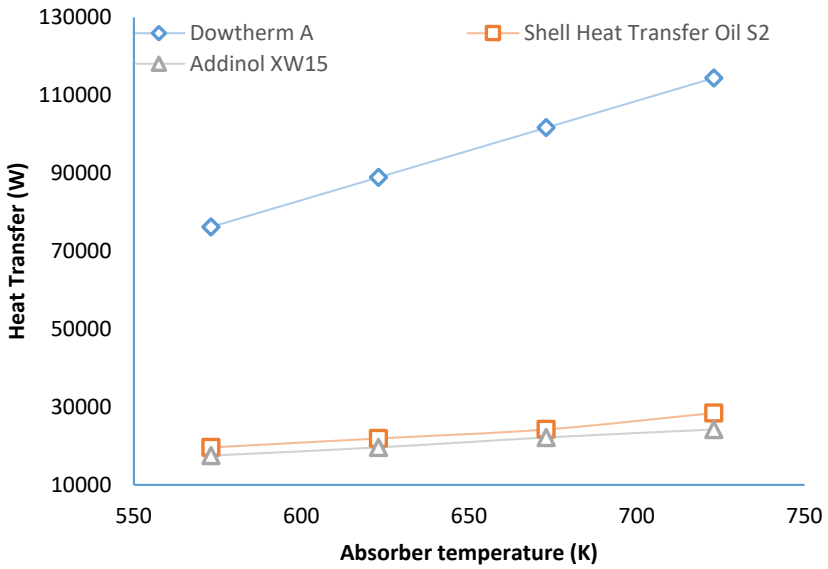

Figure 7.22. Effect of absorber wall temperature on heat transfer for mass flow rate 0.25 kg/s.

CHAPTER-VIII

8 Conclusion

- In the present study, thermal losses are presented for staggered arrangement of the trapezoidal cavity used in CLFR plant. Temperature profile is uniform in horizontal direction. At 350 K, radiation losses comprise of 62.8 % of total heat loss which is increased to 87.4 % at 550 K of absorber wall temperature. There is a significant dominance of radiation heat loss. Convection loss is almost uniform after 400 K. For coating of 0.5 emissivity, 81.5 % of total losses are radiation losses for a constant wall temperature 550 K and h=10 W/m^2K which is increased to 88.8 % for the higher value of emissivity (0.9). For constant absorber wall temperature of 550 K and emissivity 0.8, convective losses are increased from 11.7% to 14% as heat transfer coefficient is increased from 5 W/m^2K to 25 W/m^2K. For staggered arrangement, pipe number 2 (starting from symmetry) has least heat losses followed by pipe 4 (adjacent to the top wall) both being far from the glass bottom aperture. Total heat loss for pipe number 2 is 56.7 % lower than the maximum total heat loss for pipe number 3.
- In the present study, numerical three dimensional model of trapezoidal cavity used in LFR was analysed considering actual HTF flow in absorber tubes. Relative dominance of convective and radiative losses was evaluated. At lower absorber temperature (350 K) convective losses is found to be 43% of the total heat loss whereas radiative losses accounted 57%. For higher absorber temperature (550 K) radiative losses are dominant (77%) and convective losses are reduced to 23%. The cavity air temperature is used to calculate air temperature gradient for studying the effect of wind blow on lower glass plate as well as varied absorber tube temperatures. The air temperature gradient in the horizontal direction (parallel to lower glass plate) is found to be negligible whereas it is varied significantly in vertical direction (normal to lower glass plate). The average cavity air temperature is observed to be 480 K for low wind flow (h=5 W/m2K) and it reduces to 360 K for h=25 W/m2K. This has resulted in increased convective losses (27% higher).
- In the present numerical investigation, the three-dimensional trapezoidal cavity is studied for different heat transfer fluids at various inlet temperature conditions. It can be concluded that for lower inlet temperature i.e. 80°C the temperature rise is higher as compared to

200°C of inlet temperature for each fluid keeping mass flow rate 0.2 kg/s and absorber wall temperature 573 K as constant. The temperature rise is reduced from 39.72°C, 29.65°C, 26.77°C and 16.48°C for Marlotherm X, Syltherm XLT, Therminol D12 and Santotherm 59 to 18.22°C, 15.43°C, 14.81°C and 15.19°C respectively. The temperature rise is maximum for Marlotherm X at all values of inlet temperature followed by Syltherm XLT, Therminol D12 and Santotherm 59. There is 49.87% reduction in temperature rise for Marlotherm X as inlet temperature is increased from 80°C to 200°C. However, heat transfer is higher for Therminol D12 followed by Marlotherm X, Santotherm 59 and Syltherm XLT. There is 35.53% increase in heat transfer from Therminol D12 with increasing inlet temperature. Further, for the inlet temperature of 200°C least heat transfer is shown by Syltherm XLT which is 24.5% lesser than Therminol D12 at the same temperature.

- In present study, numerical analysis is carried out for a three-dimensional trapezoidal cavity used in CLFR plant with different heat transfer fluids in absorber tubes. It can be concluded that higher outlet fluid temperature is observed for addinol XW15 operated at absorber wall temperature 573 K and mass flow rate 0.1 kg/s. At low flow rate of 0.1 kg/s, the heat carrying capacity is found to be varied within 8.25%. For a flow rate of 0.2 kg/s, major increase in thermal performance of HTF is observed for Dowtherm A. For a mass flow rate of 0.2 kg/s and 0.25 kg/s turbulent characteristics are observed for Dowtherm A therefore the heat that is exchanged is significantly higher as compared to higher viscosity HTF. The increase for Dowtherm is steeper than Shell Heat Transfer Oil S2 HTF, 51.6% for mass flow rate 0.2 kg/s and 50% increase for flow rate of 0.25 kg/s which is 46.3% and 45.02% for Shell Heat Transfer Oil S2 respectively. The increase shown for Addinol XW15 is 55.47% and 38.2% approximately for mass flow rate of 0.2 kg/s and 0.25 kg/s respectively.

9 References

[1] G. Masson, M. Latour, and D. Biancardi, “Global market outlook for photovoltaics until 2016,” *Eur. Photovolt. Ind. Assoc.*, vol. 5, 2012.

[2] K. Lovegrove and W. Stein, *Concentrating solar power technology : principles, developments and applications*. Woodhead Publishing, 2012.

[3] G. Zhu, T. Wendelin, M. J. Wagner, and C. Kutscher, “History, current state, and future of linear Fresnel concentrating solar collectors,” *Sol. Energy*, vol. 103, pp. 639–652, 2014.

[4] G. Morin, J. Dersch, M. Eck, A. Häberle, and W. Platzer, “Comparison of linear Fresnel and parabolic trough collector systems—influence of linear Fresnel collector design variations on break-even cost,” in *Proc. 15th SolarPACES Conf., Berlin, Germany, 15–18 September 2009, paper 14874*, 2009.

[5] J. Burgaleta, S. Arias, and D. Ramirez, “Gemasolar, the first tower thermosolar commercial plant with molten salt storage,” in *SolarPA-CES 2012 International Conference, Marrakech, Morocco, Sept*, 2012, pp. 11–14.

[6] D. R. Mills and G. L. Morrison, “Advanced Fresnel Reflector Powerplants - Performance and Generating Costs,” *Proc. Sol. ’97*, vol. 61, no. 1968, pp. 1–9, 1997.

[7] J. Jaus, A. W. Bett, H. Reinecke, and E. R. Weber, “Reflective secondary optical elements for fresnel lens based concentrator modules,” *Prog. Photovoltaics Res. Appl.*, vol. 19, no. 5, pp. 580–590, 2011.

[8] G. Burgess, K. Lovegrove, S. Mackie, J. Zapata, and J. Pye, “Direct Steam Generation Using the SG4 500 m2 Paraboloidal Dish Concentrator,” in *Proceedings of the 17th SolarPACES Conference, Granada, Spain, Sept*, 2011, pp. 15–18.

[9] J. Badcock and M. Lenzen, “Subsidies for electricity-generating technologies: A review,” *Energy Policy*, vol. 38, no. 9, pp. 5038–5047, 2010.

[10] World Bank, “Assessment of the World Bank/GEF Strategy for the Market Development of Concentrating Solar Thermal Power,” *Rep. Prep. World Bank*, 2006.

[11] “International Energy Agency. International Energy Agency (‘IEA’) website;2016.” .

[12] A. G. Kearney, “Solar Thermal Electricity 2025, Report for ESTELLA by A.T. Kearney GmbH, Kaistraße 16A, 40221 Duesseldorf, Germany,” 2010.

[13] C. Kutscher, M. Mehos, C. Turchi, G. Glatzmaier, and T. Moss, “Line-focus solar power plant cost reduction plan,” *Contract*, vol. 303, pp. 275–3000, 2010.

[14] G. J. Kolb, C. K. Ho, T. R. Mancini, and J. A. Gary, “Power tower technology roadmap and cost reduction plan,” *SAND2011-2419, Sandia Natl. Lab. Albuquerque, NM*, vol. 7, 2011.

[15] S. H. Madaeni, R. Sioshansi, and P. Denholm, “Capacity value of concentrating solar power plants,” *Contract*, vol. 303, pp. 275–3000, 2011.

[16] R. Sioshansi and P. Denholm, “The value of concentrating solar power and thermal energy storage,” *IEEE Trans. Sustain. Energy*, vol. 1, no. 3, pp. 173–183, 2010.

[17] J. Gordon, *Solar energy: the state of the art: ISES position papers*. Earthscan, 2001.

[18] A. Bejan and G. Tsatsaronis, *Thermal design and optimization*. John Wiley & Sons, 1996.

[19] T. L. Bergman, F. P. Incropera, D. P. DeWitt, and A. S. Lavine, *Fundamentals of heat and mass transfer*. John Wiley & Sons, 2011.

[20] Y. A. Cengel, *Fluid mechanics*. Tata McGraw-Hill Education, 2010.

[21] A. Rabl and P. Bendt, “Effect of circumsolar radiation on performance of focusing collectors,” *ASME J. Sol. Energy Eng*, vol. 104, no. 3, pp. 237–250, 1982.

[22] G. Kopp and J. L. Lean, “A new, lower value of total solar irradiance: Evidence and climate significance,” *Geophys. Res. Lett.*, vol. 38, no. 1, 2011.

[23] A. B. Meinel and M. P. Meinel, *Applied Solar Energy, An Introduction, Addison-Wesley, Reading, MA*. 1976.

[24] D. Buie, A. G. Monger, and C. J. Dey, “Sunshape distributions for terrestrial solar simulations,” *Sol. energy*, vol. 74, no. 2, pp. 113–122, 2003.

[25] A. Steinfeld and M. Schubnell, “Optimum aperture size and operating temperature of a solar cavity-receiver,” *Sol. Energy*, vol. 50, no. 1, pp. 19–25, 1993.

[26] A. C. Project, “http://www.areva.com/EN/global-offer-725/concentrated- solar-power-

renewable-energies-solutions.html 2011.” .

[27] NovatecSolar, “NOVATEC SOLAR’s Website 2012,” 2012.

[28] F. Burkholder and C. F. Kutscher, *Heat-loss testing of Solel’s UVAC3 parabolic trough receiver*. Citeseer, 2008.

[29] G L Buffon, “Burning Instruments,” *The Edinburgh Encyclopaedia, D. Brewster (ed.)*. pp. 135–137, 1830.

[30] G. Francia, “Pilot plants of solar steam generating stations,” *Sol. Energy*, vol. 12, no. 1, p. 51IN359IN763-58IN562IN1364, 1968.

[31] C. Silvi, “The pioneering work on linear Fresnel reflector concentrators (LFCs) in Italy,” *Proc. SolarPACES*, 2009.

[32] W. W. Shaner and W. S. Duff, “Solar thermal electric power systems: comparison of line-focus collectors,” *Sol. Energy*, vol. 22, no. 1, pp. 49–61, 1979.

[33] D. G. Dicanio, W. J. Treytl, F. A. Jur, and C. D. Watson, “Line focus solar thermal central receiver research study,” *Final Report, 30 Apr. 1977-31 Mar. 1979 FMC Corp., St. Clara, CA. Eng. Syst. Div.*, 1979.

[34] D. Feuermann and J. M. Gordon, “Analysis of a two-stage linear Fresnel reflector solar concentrator,” *J. Sol. energy Eng.*, vol. 113, no. 4, pp. 272–279, 1991.

[35] A. Rabl and R. Winston, “Ideal concentrators for finite sources and restricted exit angles,” *Appl. Opt.*, vol. 15, no. 11, pp. 2880–2883, 1976.

[36] D. R. Mills, “Proposed solar cogeneration powerplant for 2000 Olympics,” in *Fuel and Energy Abstracts*, 1996, vol. 4, no. 37, p. 281.

[37] D. R. Mills and G. L. Morrison, “Compact linear Fresnel reflector solar thermal powerplants,” *Sol. energy*, vol. 68, no. 3, pp. 263–283, 2000.

[38] D. Mills, “WAS THE ITALIAN SOLAR ENERGY PIONEER GIOVANNI FRANCIA RIGHT?”

[39] D. R. Mills and C. J. Dey, “Transition strategies for solar thermal power generation,” *Proc.*

Int. Sol. Energy Soc. Congr. Jerusalem, 1999.

[40] C. Dey, D. R. Mills, and G. L. Morrison, “Operation of a CLFR research apparatus,” *ANZSES Annu.*, 2000.

[41] D. J. Reynolds, M. J. Jance, M. Behnia, and G. L. Morrison, “An experimental and computational study of the heat loss characteristics of a trapezoidal cavity absorber,” vol. 76, pp. 229–234, 2004.

[42] J. Smeltink, A. W. Blakers, and S. Hiron, “The ANU 20kW PV/Trough concentrator [earlier version],” 1999.

[43] Q. Zhang and D. R. Mills, “New cermet film structures with much improved selectivity for solar thermal applications,” *Appl. Phys. Lett.*, vol. 60, no. 5, pp. 545–547, 1992.

[44] A. Häberle *et al.*, “The Solarmundo Project. Advanced technology for solar thermal power generation,” in *Solar World Congress*, 2001.

[45] D. R. Mills, “Two-stage solar collectors approaching maximal concentration,” *Sol. energy*, vol. 54, no. 1, pp. 41–47, 1995.

[46] D. R. Mills, G. Morrison, J. Pye, and P. Le Lievre, “Multi-tower line focus Fresnel array project,” *J. Sol. Energy Eng.*, vol. 128, no. 1, pp. 118–120, 2006.

[47] D. R. Mills, G. L. Morrison, and P. L. Liévre, “Project Proposal for a Compact Linear Fresnel Reflector Solar Thermal Plant in the Hunter Valley,” in *ANZSES Annual Conference—Solar Harvest, Newcastle, Australia, Technical Report*, 2002.

[48] J. D. Pye, G. L. Morrison, M. Behnia, and D. Mills, “Modelling of cavity receiver heat transfer for the compact linear Fresnel reflector,” in *Proceedings of ISES Solar World Congress*, 2003.

[49] D. R. Mills, P. Le Lievre, and G. L. Morrison, “First results from compact linear Fresnel reflector installation,” *Proc. ANZSES Solar2004*, 2004.

[50] D. Mills, G. L. Morrison, and P. Le Lièvre, “Design of a 240 MWe Solar Thermal Power Plant,” *Power*, pp. 1–8, 2004.

[51] D. Mills, P. Le Lievre, and G. L. Morrison, “Lower temperature approach for very large

solar power plants," in *Proceedings of the Eurosun 2004 Conference*, 2004.

[52] M. Mertins, H. Lerchenmüller, A. Häberle, and V. Heinzel, "Geometry optimization of Fresnel-collectors with economic assessment," in *Conference Proceedings EuroSun*, 2004, pp. 1–918.

[53] M. Mendelsohn, T. Lowder, and B. Canavan, "Utility-scale concentrating solar power and photovoltaics projects: A technology and market overview," *Contract*, vol. 303, pp. 275–3000, 2012.

[54] PEM, "FNEG Solar," *Power Engineering Magazine*, p. http://www. power-com/articles/2011/03/areva-f, 2011.

[55] W. M. Conlon, P. Johnson, and R. Hanson, "Superheated steam from CLFR solar steam generators," in *ASME 2011 Power Conference collocated with JSME ICOPE 2011*, 2011, pp. 301–307.

[56] R. Bernhard *et al.*, "Linear Fresnel Collector Demonstration on the PSA. Part I—Design, Construction and Quality Control," in *14th International SolarPACES Symposium, Las Vegas, NV, Mar*, 2008, pp. 3–7.

[57] G. Morin *et al.*, "Road map towards the demonstration of a linear Fresnel collector using single tube receiver," 2006.

[58] H. T. Eck M, "Dynamics and control of parabolic trough collector loops with direct steam generation," *Sol. Energy*, vol. 81, pp. 268–279, 2007.

[59] R. Bernhard *et al.*, "Linear Fresnel collector demonstration at the PSA-operation and investigation," 2009.

[60] G. Morin, J. Dersch, W. Platzer, M. Eck, and A. Häberle, "Comparison of linear Fresnel and parabolic trough collector power plants," *Sol. Energy*, vol. 86, no. 1, pp. 1–12, 2012.

[61] Appleyard D, "Chilling in the heat of the Doha sun', Renewable Energy World," *Renew. Energy World, December*, 2010.

[62] R. Abbas, J. Muñoz-Antón, M. Valdés, and J. M. Martínez-Val, "High concentration linear Fresnel reflectors," *Energy Convers. Manag.*, vol. 72, pp. 60–68, 2013.

[63] C. Hildebrandt, “Hochtemperaturstabile Absorberschichten für linear konzentrierende solarthermische Kraftwerke,” 2009.

[64] A. Brunotte, M. P. Lazarov, and R. Sizmann, “Calorimetric measurements of the total hemispherical emittance of selective surfaces at high temperatures,” in *Optical Materials Technology for Energy Efficiency and Solar Energy*, 1992, pp. 149–160.

[65] C. E. Kennedy, *Review of mid-to high-temperature solar selective absorber materials*, vol. 1617. National Renewable Energy Laboratory Golden, Colo, USA, 2002.

[66] S. Brunold, U. Frei, B. Carlsson, K. Möller, and M. Köhl, “Accelerated life testing of solar absorber coatings:: Testing procedure and results,” *Sol. Energy*, vol. 68, no. 4, pp. 313–323, 2000.

[67] O. P. Agnihotri and B. K. Gupta, “Solar selective surfaces,” *New York, Wiley-Interscience, 1981. 232 p.*, 1981.

[68] Q.-C. Zhang, “Recent progress in high-temperature solar selective coatings,” *Sol. Energy Mater. Sol. Cells*, vol. 62, no. 1, pp. 63–74, 2000.

[69] E. Randich and D. D. Allred, “Chemically vapor-deposited ZrB 2 as a selective solar absorber,” *Thin Solid Films*, vol. 83, no. 4, pp. 393–398, 1981.

[70] J. J. Cuomo, J. F. Ziegler, and J. M. Woodall, “A new concept for solar energy thermal conversion,” *Appl. Phys. Lett.*, vol. 26, no. 10, pp. 557–559, 1975.

[71] S. Zhao, “Spectrally selective solar absorbing coatings prepared by dc magnetron sputtering.” Acta Universitatis Upsaliensis, 2007.

[72] C. G. Granqvist and C. G. Granqvist, *Renewable Energy Series: Materials Science for Solar Energy Conversion Systems*. Pergamon Press, Oxford, UK, 1991.

[73] D. R. Mills, A. Monger, and G. L. Morrison, “Comparison of fixed asymmetrical and symmetrical reflectors for evacuated tube solar receivers,” *Sol. Energy*, vol. 53, no. 1, pp. 91–104, 1994.

[74] W. M. Conlon, P. M. Tanner, M. Venetos, and R. J. Hanson, “Systems and methods for producing steam using solar radiation.” Google Patents, 14-May-2010.

[75] C. Sella, A. Bichri, J. C. Martin, J. Lafait, K. Driss-Khodja, and S. Berthier, “Adjustable optical properties of coatings based on cermet thin films near the percolation threshold,” *Phys. A Stat. Mech. its Appl.*, vol. 157, no. 1, pp. 555–560, 1989.

[76] T. E. Graedel, “Corrosion mechanisms for silver exposed to the atmosphere,” *J. Electrochem. Soc.*, vol. 139, no. 7, pp. 1963–1970, 1992.

[77] Q. Zhang and D. R. Mills, “Very low-emittance solar selective surfaces using new film structures,” *J. Appl. Phys.*, vol. 72, no. 7, pp. 3013–3021, 1992.

[78] J. A. Thornton, A. S. Penfold, and J. L. Lamb, “Sputter-deposited Al 2 O 3/Mo/Al 2 O 3 selective absorber coatings,” *Thin Solid Films*, vol. 72, no. 1, pp. 101–110, 1980.

[79] D. R. Mills, P. Le Lièvre, and G. L. Morrison, “First Results from Compact Linear Fresnel Reflector Installation,” *Power*, pp. 1–7, 2000.

[80] D. J. Reynolds, M. Behnia, and G. L. Morrison, “A Hydrodynamic Model for a Line-Focus Direct Steam Generation Solar Collector,” *Sol. 2002*, pp. 1–6, 2002.

[81] S. A. Kalogirou, *Solar thermal collectors and applications*, vol. 30. 2004.

[82] D. Mills, “Advances in solar thermal electricity technology,” *Sol. Energy*, vol. 76, no. 1–3, pp. 19–31, 2004.

[83] D. R. Mills and G. L. Morrison, “Compact Linear Fresnel Reflector Solar Thermal Power Plants,” vol. 68, no. 3, pp. 263–283, 2006.

[84] C. J. Dey, “Heat transfer aspects of an elevated linear absorber,” vol. 76, no. 2004, pp. 243–249, 2006.

[85] J. Pye, G. Morrison, and M. Behnia, “Pressure Drops for Direct Steam Generation in In-Line Focus Solar Thermal Systems,” … *Aust. New Zeal. Sol. …*, no. Romero 2002, 2006.

[86] J. D. Pye, G. L. Morrison, and M. Behnia, “Unsteady effects in direct steam generation in the CLFR,” *Anzses*, pp. 1–9, 2007.

[87] C. Kennedy, “Advances in concentrating solar power collectors: mirrors and solar-selective coatings,” *Vac. Tech. Coat.*, vol. 6103, no. October, 2008.

[88] P. L. Singh, R. M. Sarviya, and J. L. Bhagoria, “Thermal performance of linear Fresnel reflecting solar concentrator with trapezoidal cavity absorbers,” *Appl. Energy*, vol. 87, no. 2, pp. 541–550, 2010.

[89] J. Fac??o and A. C. Oliveira, “Numerical simulation of a trapezoidal cavity receiver for a linear Fresnel solar collector concentrator,” *Renew. Energy*, vol. 36, no. 1, pp. 90–96, 2011.

[90] R. Abbas, J. Muñoz, and J. M. Martínez-Val, “Steady-state thermal analysis of an innovative receiver for linear Fresnel reflectors,” *Appl. Energy*, vol. 92, pp. 503–515, 2012.

[91] S. K. Natarajan, K. S. Reddy, and T. K. Mallick, “Heat loss characteristics of trapezoidal cavity receiver for solar linear concentrating system,” *Appl. Energy*, vol. 93, no. May, pp. 523–531, 2012.

[92] S. Flores Larsen, M. Altamirano, and A. Hernández, “Heat loss of a trapezoidal cavity absorber for a linear Fresnel reflecting solar concentrator,” *Renew. Energy*, vol. 39, no. 1, pp. 198–206, 2012.

[93] S. S. Sahoo, S. Singh, and R. Banerjee, “Analysis of heat losses from a trapezoidal cavity used for Linear Fresnel Reflector system,” *Sol. Energy*, vol. 86, no. 5, pp. 1313–1322, 2012.

[94] M. Lin, K. Sumathy, Y. J. Dai, R. Z. Wang, and Y. Chen, “Experimental and theoretical analysis on a linear Fresnel reflector solar collector prototype with V-shaped cavity receiver,” *Appl. Therm. Eng.*, vol. 51, no. 1–2, pp. 963–972, 2013.

[95] S. S. Sahoo, S. Singh, and R. Banerjee, “Steady state hydrothermal analysis of the absorber tubes used in Linear Fresnel Reflector solar thermal system,” *Sol. Energy*, vol. 87, no. 1, pp. 84–95, 2013.

[96] K. S. Reddy and K. R. Kumar, “International Journal of Thermal Sciences Estimation of convective and radiative heat losses from an inverted trapezoidal cavity receiver of solar linear Fresnel re fl ector system,” *Int. J. Therm. Sci.*, vol. 80, pp. 48–57, 2014.

[97] I. F. Okafor, J. Dirker, and J. P. Meyer, “Influence of circumferential solar heat flux distribution on the heat transfer coefficients of linear Fresnel collector absorber tubes,” *Sol. Energy*, vol. 107, pp. 381–397, 2014.

[98] J. Zhu and H. Huang, “Design and thermal performances of Semi-Parabolic Linear Fresnel Reflector solar concentration collector,” *Energy Convers. Manag.*, vol. 77, pp. 733–737, 2014.

[99] M. A. Moghimi, K. J. Craig, and J. P. Meyer, “Optimization of a trapezoidal cavity absorber for the Linear Fresnel Reflector,” *Sol. Energy*, vol. 119, pp. 343–361, 2015.

[100] A. Saxena, N. Jhamaria, S. Singh, and S. S. Sahoo, “Numerical analysis of convective and radiative heat losses from trapezoidal cavity receiver in LFR systems,” *Sol. Energy*, vol. 137, pp. 308–316, 2016.

[101] H. Beltagy, D. Semmar, C. Lehaut, and N. Said, “Theoretical and experimental performance analysis of a Fresnel type solar concentrator,” *Renew. Energy*, vol. 101, pp. 782–793, 2017.

[102] J. . Pye, “System Modelling of the Compact Linear Fresnel Reflector,” University of New South Wales, Australia, 2008.

[103] Y. Lai *et al.*, “Thermal performance analysis of linear fresnel reflector concentrator with a compound parabolic cavity absorber,” *ICMREE2011 - Proc. 2011 Int. Conf. Mater. Renew. Energy Environ.*, vol. 1, pp. 168–172, 2011.

[104] A. C. Facaˆo, J., Oliveira, “Numerical simulation of a trapezoidal cavity receiver for a linear Fresnel solar collector concentrator,” *Renew. Energy*, vol. 36, pp. 90–96, 2011.

[105] ANSYS 2013a, “Ansys Fluent Help.” ANSYS Incorporated, 2013.

[106] A. Bakker, “Lecture 7-Meshing Applied Computational Fluid Dynamics,” 2002.

[107] C. Haberle, A., Zahler, C., Lerchenmuller, H., Mertins, M., Wittwer and J. Trieb, F., Dersch, “The solarmundo line focussing Fresnel collector optical and thermal performance and cost calculations,” in *11th SolarPACES Conference*, 2002.

[108] A. Heimsath, F. Cuevas, A. Hofer, P. Nitz, and W. J. Platzer, “Linear Fresnel Collector receiver: Heat loss and temperatures,” *Energy Procedia*, vol. 49, pp. 386–397, 2013.

[109] M. A. Moghimi, K. J. Craig, and J. P. Meyer, “Optimization of a trapezoidal cavity absorber for the Linear Fresnel Reflector,” *Sol. Energy*, vol. 119, pp. 343–361, 2015.

[110] D. D. Gray and A. Giorgini, “The validity of the Boussinesq approximation for liquids and

gases," *Int. J. Heat Mass Transf.*, vol. 19, no. 5, pp. 545–551, 1976.

[111] L. Amsbeck, R. Buck, P. Heller, J. Jedamski, and R. Uhlig, "Development of a tube receiver for a solar-hybrid microturbine system," in *Proceedings of the 14th Biennial CSP Solarpaces Symposium 2008*, 2008.

[112] R. W. BRADSHAW *et al.*, "Final test and evaluation results from the solar two project," Sandia National Labs., Albuquerque, NM (US); Sandia National Labs., Livermore, CA (US), 2002.

[113] G. Hughes *et al.*, "Reduction of convective losses in solar cavity receivers," *AIP Conf. Proc.*, vol. 1734, 2016.

[114] H. Benoit, I. P. López, D. Gauthier, J.-L. Sans, and G. Flamant, "On-sun demonstration of a 750° C heat transfer fluid for concentrating solar systems: dense particle suspension in tube," *Sol. Energy*, vol. 118, pp. 622–633, 2015.

[115] G. Flamant *et al.*, "Dense suspension of solid particles as a new heat transfer fluid for concentrated solar thermal plants: on-sun proof of concept," *Chem. Eng. Sci.*, vol. 102, pp. 567–576, 2013.

[116] M. J. Bignon, "The influence of the heat transfer fluid on the receiver design," *Electr. Power Syst. Res.*, vol. 3, no. 1–2, pp. 99–109, 1980.

[117] Ho CK, "Computational fluid dynamics for concentrating solar power systems," *Wiley Interdiscip. Rev. Energy Environ.*, 2013.

[118] A. Bakker, "Lecture 7 – Meshing," in *Applied Computational Fluid Dynamics*, 2013.

[119] J. G. Cordaro, N. C. Rubin, and R. W. Bradshaw, "Multicomponent molten salt mixtures based on nitrate/nitrite anions," *J. Sol. Energy Eng.*, vol. 133, no. 1, p. 11014, 2011.

[120] J. Pacio and T. Wetzel, "Assessment of liquid metal technology status and research paths for their use as efficient heat transfer fluids in solar central receiver systems," *Sol. Energy*, vol. 93, pp. 11–22, 2013.

[121] Y. Tian and C.-Y. Zhao, "A review of solar collectors and thermal energy storage in solar thermal applications," *Appl. Energy*, vol. 104, pp. 538–553, 2013.

[122] A. Gil *et al.*, “State of the art on high temperature thermal energy storage for power generation. Part 1—Concepts, materials and modellization,” *Renew. Sustain. Energy Rev.*, vol. 14, no. 1, pp. 31–55, 2010.

[123] K. Vignarooban, X. Xu, A. Arvay, K. Hsu, and A. M. Kannan, “Heat transfer fluids for concentrating solar power systems–a review,” *Appl. Energy*, vol. 146, pp. 383–396, 2015.

[124] A. Modi and F. Haglind, “Performance analysis of a Kalina cycle for a central receiver solar thermal power plant with direct steam generation,” *Appl. Therm. Eng.*, vol. 65, no. 1, pp. 201–208, 2014.

[125] D. N. Nkwetta, M. Smyth, A. Zacharopoulos, and T. Hyde, “Experimental performance analysis and optimisation of medium temperature solar thermal collectors with silicon oil as a heat transfer fluid,” *Int. J. Energy Res.*, vol. 37, no. 6, pp. 570–581, 2013.

[126] M. Ouagued, A. Khellaf, and L. Loukarfi, “Estimation of the temperature, heat gain and heat loss by solar parabolic trough collector under Algerian climate using different thermal oils,” *Energy Convers. Manag.*, vol. 75, pp. 191–201, 2013.

[127] M. Collares-Pereira, D. Canavarro, and L. L. Guerreiro, “15 - Linear Fresnel reflector (LFR) plants using superheated steam, molten salts, and other heat transfer fluids A2 - Blanco, Manuel J.,” in *Woodhead Publishing Series in Energy*, L. R. B. T.-A. in C. S. T. R. and T. Santigosa, Ed. Woodhead Publishing, 2017, pp. 339–352.

[128] S. Sau *et al.*, “Techno-economic comparison between CSP plants presenting two different heat transfer fluids,” *Appl. Energy*, vol. 168, pp. 96–109, Apr. 2016.

[129] R. Gardon and J. C. Akfirat, “The role of turbulence in determining the heat-transfer characteristics of impinging jets,” *Int. J. Heat Mass Transf.*, vol. 8, no. 10, pp. 1261–1272, 1965.

[130] J. C. Hart, J. S. Park, and C. K. Lei, “Heat transfer enhancement in channels with turbulence promoters,” *J. Eng. Gas Turbines Power*, vol. 107, pp. 628–635, 1985.

[131] S. Pethkool, S. Eiamsa-Ard, S. Kwankaomeng, and P. Promvonge, “Turbulent heat transfer enhancement in a heat exchanger using helically corrugated tube,” *Int. Commun. Heat Mass Transf.*, vol. 38, no. 3, pp. 340–347, 2011.

[132] A. Garcia, P. G. Vicente, and A. Viedma, “Experimental study of heat transfer enhancement with wire coil inserts in laminar-transition-turbulent regimes at different Prandtl numbers,” *Int. J. Heat Mass Transf.*, vol. 48, no. 21, pp. 4640–4651, 2005.